AD_____

Award Number: DAMD17-03-1-0729

TITLE: Healing of Stress Fracture in an Animal Model

PRINCIPAL INVESTIGATOR: Jiliang Li, M.D., Ph.D.

CONTRACTING ORGANIZATION: Indiana University
Indianapolis, IN 46202-5167

REPORT DATE: September 2005

TYPE OF REPORT: Final

PREPARED FOR: U.S. Army Medical Research and Materiel Command
Fort Detrick, Maryland 21702-5012

DISTRIBUTION STATEMENT: Approved for Public Release;
Distribution Unlimited

REPORT DOCUMENTATION PAGE

Form Approved
OMB No. 0704-0188

1. REPORT DATE *(DD-MM-YYYY)*	2. REPORT TYPE	3. DATES COVERED *(From - To)*
01-09-2005	Final	1 Sep 03 – 31 Aug 05

4. TITLE AND SUBTITLE
Healing of Stress Fracture in an Animal Model

5a. CONTRACT NUMBER

5b. GRANT NUMBER
DAMD17-03-1-0729

5c. PROGRAM ELEMENT NUMBER

6. AUTHOR(S)
Jiliang Li, M.D., Ph.D.

E-Mail: jilili@iupui.edu

5d. PROJECT NUMBER

5e. TASK NUMBER

5f. WORK UNIT NUMBER

7. PERFORMING ORGANIZATION NAME(S) AND ADDRESS(ES)

Indiana University
Indianapolis, IN 46202-5167

8. PERFORMING ORGANIZATION REPORT NUMBER

9. SPONSORING / MONITORING AGENCY NAME(S) AND ADDRESS(ES)
U.S. Army Medical Research and Materiel Command
Fort Detrick, Maryland 21702-5012

10. SPONSOR/MONITOR'S ACRONYM(S)

11. SPONSOR/MONITOR'S REPORT NUMBER(S)

12. DISTRIBUTION / AVAILABILITY STATEMENT
Approved for Public Release; Distribution Unlimited

13. SUPPLEMENTARY NOTES

14. ABSTRACT

This project aimed to develop effective ways to prevent or treat stress fractures. We have investigated the role of an exercise program in the prevention of stress fractures using the ulna axial compression loading model. Loading was applied on right ulnas using a 2-Hz haversine waveform with a peak force of 17 N for 360 cycles/day, three days per week for five consecutive weeks. Exercise loading improved structural properties of the ulna, especially minimum second moment of area increasing about 2-fold. However, the exercise program increased the fatigue resistance by 100-fold. In addition, We studied the individual and combined roles of anti-inflammatory agent (cyclooxygenase-2 inhibitor, celebrex) and low-intensity pulsed ultrasound (LIPUS) in the treatment of stress fractures. Our data indicates that LIPUS has a beneficial and celebrex has a detrimental effect on stress fracture repair. While neither LIPUS or celebrex influenced bone resorption, both had significant effects on intracortical bone formation. These effects were opposing, and indicate that LIPUS may be used to facilitate stress fracture repair whereas celebrex may delay tissue level repair of stress fractures. There were no interactions between LIPUS and celebrex, indicating that the beneficial LIPUS effect was not mediated by a COX-2 pathway. These findings have implications for the clinical utility of these interventions in the management of stress fractures.

15. SUBJECT TERMS
Stress fracture, exercise, loading, cyclooxygenase-2 inhibitor, therapeutic ultrasound, animal model

16. SECURITY CLASSIFICATION OF:			17. LIMITATION OF ABSTRACT	18. NUMBER OF PAGES	19a. NAME OF RESPONSIBLE PERSON
a. REPORT	b. ABSTRACT	c. THIS PAGE			USAMRMC
U	U	U	UU	29	19b. TELEPHONE NUMBER *(include area code)*

Table of Contents

Introduction

This project originally aimed to develop effective ways to prevent or treat stress fractures. The original project includes 2 studies:

1. Bone adaptation to a mechanical loading program significantly increases skeletal fatigue resistance.
2. Effect of low intensity pulsed ultrasound and a cycloxygenase-2 inhibitor on stress fracture repair.

New study was also developed based on this project:

1. Imaging bone microdamage in vivo with positron emission tomography.

Study one: Bone adaptation to a mechanical loading program significantly increases skeletal fatigue resistance (JBMR 2005; 20:809-816 with Title shown on the cover)

Site-specific mechanical loading was performed on one forearm of adult female Sprague-Dawley rats using the axial compression loading model. Loading was performed 3 days/week for 5 consecutive weeks to induce adaptation. The loaded and nonloaded ulnas in each animal were removed after the loading program, and their material and structural properties were determined. The ulna pairs were subsequently loaded until fatigue failure at the same constant peak axial load.

Mechanical loading induced consistent and predictable changes in the structural properties of loaded ulnas, with the largest change being a nearly 2-fold increase in midshaft minimum second moment of area (I_{MIN}) (**Figure 1**). The mechanical-loading induced bone changes resulted in a >100-fold increase in fatigue resistance in loaded ulnas, with resistance being exponentially related to the structural properties of the ulna (**Figure 2**).

This study found that by enhancing the structural properties of a bone through a mechanical loading program, its fatigue resistance could be significantly improved. This indicates that an exercise program aimed at modifying bone structure may be used as a possible prevention strategy for stress fractures.

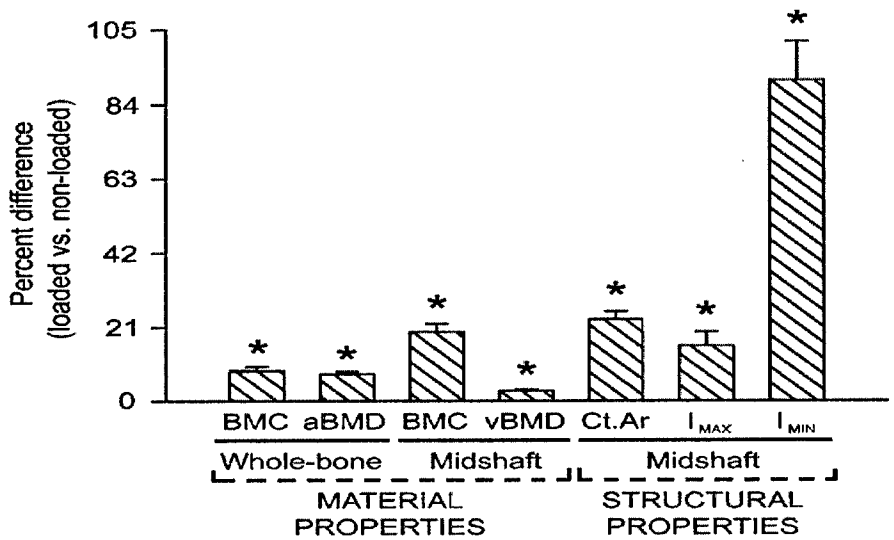

Fig. 1. Bone adaptation in response to the mechanical loading program. Bars represent the mean percent difference between the loaded and nonloaded ulnas for all animals ($N = 24$). *Significantly different from 0% (no difference between loaded and nonloaded ulnas; $p < 0.01$, single sample t-test with population mean of 0%). Error bars represent ± SD.

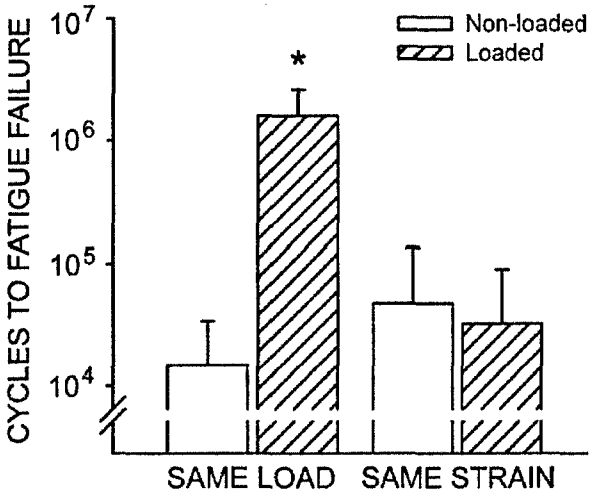

Fig. 2. Effect of bone adaptation on skeletal fatigue resistance. Cycles to fatigue failure is plotted on a log scale. *Significantly different from nonloaded ($p <$ 0.001, paired *t*-test). Error bars represent ± SD.

Study two: Effect of low intensity pulsed ultrasound and a cycloxygenase-2 inhibitor on stress fracture repair (submitted to ORS 2006)

Bilateral stress fractures were induced in the ulnas of 48 adult female Sprague-Dawley rats. Rats were anaesthetized with an intramuscular injection of ketamine hydrochloride (50 mg/kg) and xylazine (10 mg/kg). One bout of axial compressive loading was applied on ulnas using a load-controlled electromagnetic device. Loading had a peak magnitude of 17- 20 N (~3600 microstrain at mid-ulna) which was introduced at a frequency of 2 Hz for 4000-6000 cycles. The loading was stopped when the displacement increased 10% (equivalent to 10% loss of stiffness), as monitored using a CCD Laser Displacement Sensor.

Beginning the first day following stress fracture induction, half of the animals were given celebrex (a specific COX-2 inhibitor) by gavage at a dose of 4 mg/kg/day. The remaining animals were given vehicle (polyethylene glycol solution). In addition, all animals had their forelimbs shaved, and were treated unilaterally with active-LIPUS (active ultrasound) and contralaterally with inactive-LIPUS (placebo) while animals were anaesthetized using isoflurane inhalation (1-3%). Active-LIPUS consist of a 200-μs burst of 1.5-MHz sine waves repeating at 1-kHz. The I_{SATA} was set at 100 mW/cm^2. Active- and inactive-LIPUS was coupled with the skin using standard ultrasound gel and was introduced daily for 20-minutes. Therefore, a total of 4 groups were generated based on the combinations of celebrex and LIPUS treatments: Vehicle, Vehicle+LIPUS, Celebrex and Celebrex+LIPUS groups. Equal numbers of animals from each group were sacrificed at 2, 4 and 8 weeks following stress fracture induction. Three and nine days prior to sacrifice intraperitoneal injections of calcein (7 mg/kg, Sigma Chemical Co., St. Louis, MO) were administered. Following sacrifice, ulnas were dissected free and bone mineral content and density were measured using a PIXImus densitometer. The ulnas were then

prepared for histological analysis using *en bloc* basic fuchsin staining. Histomorphometric measurements were performed on cross sections of the midshaft ulna.

Periosteal woven bone formation on the periosteal surface resulted from fatigue loading. There was no difference in woven bone area or bone mineral density among all the groups (**Figure 3**). Cracks were seen in the cortex of all ulnas and there was no difference in crack length among the groups. Bone resorption spaces around the crack were seen in all the ulnas at 2 weeks following fatigue loading (**Figure 4**). The maximum area of introcortical resorption spaces was found at 4 weeks. The sizes of resorption spaces decreased significantly at 8 weeks in all groups. There was no difference in area of resorption spaces at each time point among the groups.

There were no significant interactions between LIPUS and celebrex on intracortical bone formation rate (BFR) at any time point (all $p > 0.05$, **Figure 5**). However, at 4 and 8 weeks there was a significant LIPUS main effect on BFR (all $p < 0.05$), indicating a beneficial LIPUS effect. There was no main effect for celebrex at 4 weeks; however, such an effect existed at 8 weeks, indicating that celebrex significantly reduced BFR.

This study indicates that LIPUS has a beneficial and celebrex has a detrimental effect on stress fracture repair. While neither LIPUS or celebrex influenced bone resorption, both had significant effects on intracortical BFR. These effects were opposing, and indicate that LIPUS may be used to facilitate stress fracture repair whereas celebrex may delay tissue level repair of stress fractures. There were no interactions between LIPUS and celebrex, indicating that the beneficial LIPUS effect was not mediated by a COX-2 pathway. These findings have implications for the clinical utility of these interventions in the management of stress fractures.

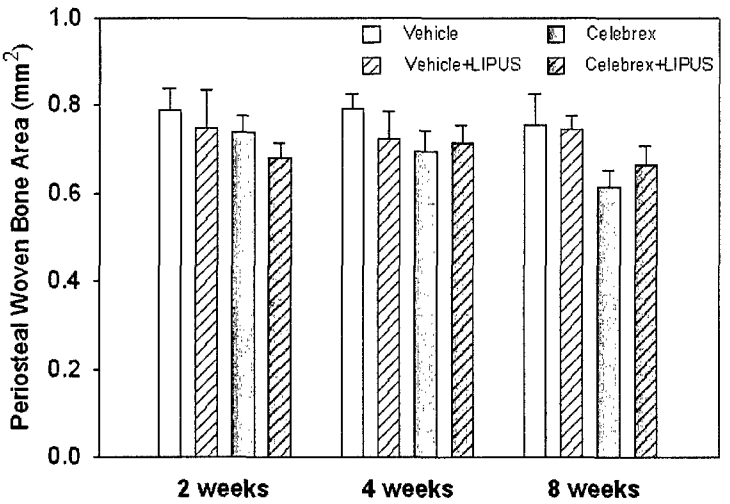

Figure 3. Area of woven bone formed in response to fatigue loading was not different among groups.

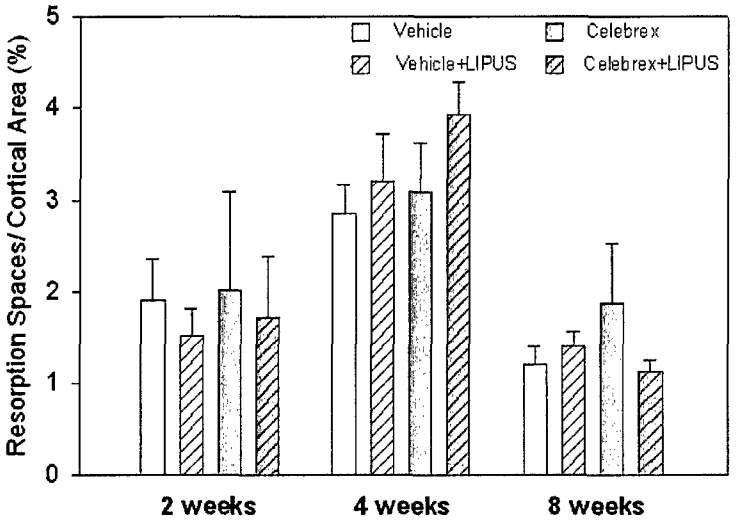

Figure 4. Intracortical bone resorption increased significantly in all groups until 4 weeks after production of bone cracks, but then decrease at 8 weeks. No difference was seen among the groups at each time point.

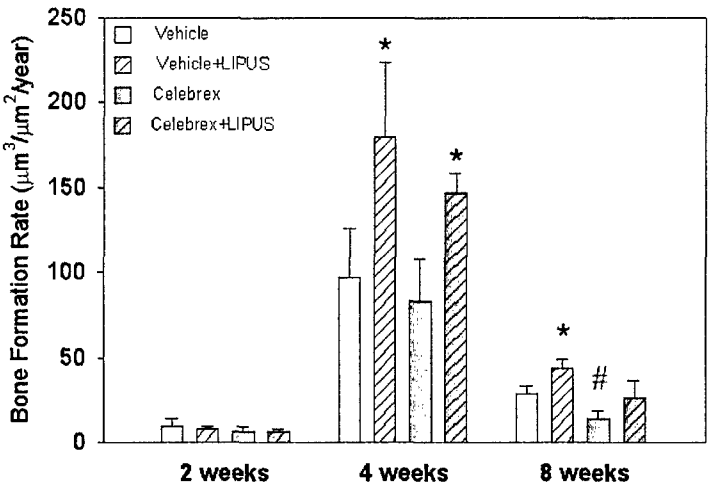

Figure 5. LIPUS significantly enhanced intracortical bone formation rate in the cortex during stress fracture repair (* $p < 0.05$ vs. Vehicle or Celebrex) at 4 and 8 weeks. Celebrex decreased bone formation (# $p < 0.05$ vs. Vehicle) at 8 weeks.

Study 3: Imaging bone microdamage in vivo with positron emission tomography (In press, Bone)

Microdamage accumulation in bone is now considered a contributing cause for bone fragility in older women. However, there is still no method to detect and quantify microdamage *in vivo*. We have found that positron emission tomography (PET) may be useful to detect and quantify bone microdamage in vivo using a high-resolution PET scanner with [^{18}F]NaF as the tracer. We have done several experiments using the rat ulnar loading model that demonstrate that (1) High-resolution [^{18}F]NaF PET can detect newly created microdamage *in vivo;* (2) the microdamage detected in this way is co-localized with damage detected by histological and autoradiographic procedures; and (3) High-resolution [^{18}F]NaF PET can distinguish between the effects of mechanical loading that does not produce damage, and fatigue loading that creates microdamage. The high-resolution [^{18}F]NaF PET shows promise as a non-invasive means to image bone microdamage.

Key Research Accomplishments
(See Appendices for the original copies)

Manuscripts:

1. **Li J**, Miller MA, Hutchins GD, Burr DB 2005 Imaging bone microdamage in vivo with positron emission tomography (in press, Bone)
2. Warden SJ, Hurst JA, Sanders MS, Turner CH, Burr DB, **Li J** 2005 Bone adaptation to a mechanical loading program significantly increased skeletal fatigue resistance. J Bone Miner Res 20(5):809-16. (**TITLE ON COVER**)

Abstracts:

3. Warden SJ, Hurst JA, Sanders MS, Turner CH, Burr DB, **Li J** 2005 Exercise-induced Bone Adaptation Significantly Increases Skeletal Fatigue Resistance. Medicine & Science in Sports & Exercise 37(5): S452.
4. Warden SJ, Hurst JA, Sanders MS, Turner CH, Burr DB, **Li J** 2005 Bone adaptation to a mechanical loading program significantly increases skeletal fatigue resistance. *Trans Orthop Res Soc 30:* In 51st annual meeting of Orthopaedic Research Society, Washington D. C. 2/20-23/05.
5. **Li J,** Warden SJ, Waugh L, Burr DB 2006 Effect of low intensity pulsed ultrasound and a cycloxygenase-2 inhibitor on stress fracture repair. Submitted to the 51st annual meeting of Orthopaedic Research Society, Chicago 2006

Reportable outcomes

1. Rodent ulnar axial compression loading model was established;
2. Two college students supported by this award took part in the project.
3. Presentation in 51st annual meeting of Orthopaedic Research Society, Washington D. C. 2/20-23, 2005.
4. Presentation in the 52nd annual meeting of Medicine & Science in Sports & Exercise 37(5): S452, 2005

Conclusions

Based on the project, the conclusions are summarized as below:

1. Bone adaptation to a mechanical loading program significantly increases skeletal fatigue resistance.
2. Effect of low intensity pulsed ultrasound and a cycloxygenase-2 inhibitor on stress fracture repair.
3. Imaging bone microdamage in vivo with positron emission tomography.

ELSEVIER

Bone xx (2005) xxx–xxx

BONE

www.elsevier.com/locate/bone

Imaging bone microdamage in vivo with positron emission tomography

Jiliang Li [a,*], Michael A. Miller [c], Gary D. Hutchins [c], David B. Burr [a,b]

[a] Department of Anatomy and Cell Biology, Indiana University School of Medicine, 635 Barnhill Drive, MS 5035, Indianapolis, IN 46202, USA
[b] Department of Orthopaedic Surgery, Indiana University School of Medicine, Indianapolis, IN 46202, USA
[c] Department of Radiology, Indiana University School of Medicine, Indianapolis, IN 46202, USA

Received 22 March 2005; revised 24 May 2005; accepted 3 June 2005

Abstract

Microdamage accumulation in bone is now considered a contributing cause for bone fragility in older women. However, there is still no method to detect and quantify microdamage in vivo. We have found that positron emission tomography (PET) may be useful to detect and quantify bone microdamage in vivo using a high-resolution PET scanner with [^{18}F]NaF as the tracer. We have done several experiments using the rat ulnar loading model that demonstrate that (1) high-resolution [^{18}F]NaF PET can detect newly created microdamage in vivo; (2) the microdamage detected in this way is co-localized with damage detected by histological and autoradiographic procedures; and (3) high-resolution [^{18}F]NaF PET can distinguish between the effects of mechanical loading that does not produce damage and fatigue loading that creates microdamage. The high-resolution [^{18}F]NaF PET shows promise as a non-invasive means to image bone microdamage.

Keywords: Bone microdamage; Positron emission tomography; Fatigue loading; Sodium fluoride; Rat ulna

Introduction

Microdamage accumulation in bone is now considered a contributing cause for bone fragility in older women [4,5]. Standard techniques for identifying microdamage histologically rely on en bloc staining with a variety of agents such as basic fuchsin [6,7], fluorescein [26], mineralized bone stain or gallocyanin [25]. Lead uranyl acetate can be used for imaging damage with electron microscopy [20]. It is also possible to use multiple fluorescent agents to detect microdamage before and after a damage event in vitro [12].

However, there is still no method to detect and quantify bone microdamage in vivo. Quantitative ultrasound is highly correlated with bone density and elastic modulus in non-damaged bone, but it cannot detect changes in elastic modulus that occur as the result of damage in vivo [1,15].

Recently, we have found that positron emission tomography (PET) may be useful to detect and quantify bone microdamage in vivo using our IndyPET-II scanner with [^{18}F]NaF as the tracer [19]. PET has the ability to image biochemical (metabolic) changes in the body by detection of regional concentrations of radioactivity in a particular organ. A radioactive isotope (tracer) is produced in an accelerator (a cyclotron) and attached, or tagged, to a biologically active compound. This biologically active compound is administered to patients or animals, and its fate in vivo is monitored by the detection of 511 keV photons produced when an emitted positron interacts with an electron in the surrounding material. The PET scanner detects the emission of paired gamma rays and forms an image of the tracer distribution within the body. Using mathematical models, the kinetics of tracer accumulation and washout in tissues can be used to quantify biological processes such as blood flow, metabolism and protein expression.

[^{18}F]NaF is used as a skeletal imaging agent in PET to delineate areas of abnormal osteogenesis. The fluoride ion becomes incorporated into bone as a result of an ion exchange (with hydroxyl ions) at the surface of the hydroxyapatite crystal [9,11,16,21]. Fluoride F-18 is taken up in bone in proportion to blood flow and bone metabolic activity [21]. It is also used to assess changes in bone metabolism, blood flow and osteoblastic activity [3,11]. We hypothesized that PET imaging of Na^{18}F uptake and retention can be used to visualize and measure the accumulated burden of microdamage at local sites of clinical importance for fracture.

* Corresponding author. Fax: +1 317 278 2040.
E-mail address: jilili@iupui.edu (J. Li).

8756-3282/$ - see front matter © 2005 Published by Elsevier Inc.
doi:10.1016/j.bone.2005.06.022

We used a well-established rat ulna loading model to induce bone microdamage [2,23]. We applied high-resolution $Na^{18}F$ PET to image microdamage in vivo in the rat model and compare the damaged and non-damaged regions with histological and autoradiographic findings made on bone stained en bloc in basic fuchsin [6].

Materials and methods

Experimental animals

Adult female Sprague–Dawley rats were used for this study. The rats were housed one per cage at the Laboratory Animal Resource Center (LARC) of Indiana University School of Medicine and were fed standard rat chow and water ad libitum. The animals were allowed to acclimate for 1 week before the experiment began and were approximately 6 months old at the beginning of the study. All procedures performed in this study were in accordance with the Indiana University Animal Care and Use Committee Guidelines.

PET imaging

Tracer preparation

[F-18] Sodium fluoride preparation: Enriched [O-18] water was irradiated with protons to form [F-18] via the reaction $^{18}O(p, n)^{18}F$. The irradiated H_2O will be passed over an anion exchange membrane. Fluorine-18 was eluted from the membrane with 3.5 mg of $KHCO_3$ dissolved in 700 μl of water. The elute was neutralized and passed over a sterile 0.22-μm filter and prepared for injection.

PET imaging protocol

Animals were anesthetized with a mixture of ketamine hydrochloride (50 mg/kg, Fort Dodge Animal Health, Fort Dodge, Iowa, USA) and xylazine (10 mg/kg, The Butler Company, Columbus, Ohio, USA), while they were being scanned using PET. The animals were imaged using a small field-of-view PET scanner (IndyPET-II), with an image resolution of approximately 2.5 mm FWHM (full width half maximum). Each subject was positioned in the PET scanner, and a transmission scan was acquired to correct the measured emission data for attenuation. Approximately 1.5–2.0 mCi of sodium fluoride ($[^{18}F]NaF$) was injected into a tail vein as a bolus, and list mode data were acquired for 1 h. Following data acquisition, the list mode data were binned into a temporal series of images (12 frames × 5 s, 6 × 10 s, 3 × 60 s, 11 × 300 s).

Imaging analysis

Attenuation-corrected images were reconstructed in a standard filtered backprojection algorithm using a Hanning filter with a cutoff frequency of 0.35 cycles per pixel. The image data from the last 55 min post-injection was integrated to form a high-quality image volume for definition of regions of interest. Regions of interest (ROI) were manually defined on the PET images in bone. We standardized (normalized) the PET imaging intensity for quantitative data analysis. The standardized PET intensity is calculated as [^{18}F] density within a region of interest (ROI) divided by the intensity within the muscle of the forearm.

Ulna fatigue loading model

Animals were anesthetized with an intramuscular injection of a mixed solution of ketamine hydrochloride and xylazine while they were loaded. Load was applied to a peak load of 17–20 N at 2 Hz using a load-controlled, electromagnetic loading device. Total loading cycles were adjusted through the connected load controller. Stiffness loss during the loading procedure was observed through continuous monitoring of displacement of the arm on the loading device using a CCD Laser Displacement Sensor (LK Series, Keyence Corp., Osaka, Japan).

Tissue preparation

All the rats were sacrificed by inhalation of CO_2 after PET scanning and the ulnae dissected out bilaterally. Specimens for histological microdamage analysis by basic fuchsin staining were fixed for 3 days in cold 10% neutral-buffered formalin. Specimens were bulk stained in two changes each of 1% basic fuchsin in 70, 80, 90 and 100% ETOH under vacuum at 15–20 in Hg for 4 h. Following staining, the bone was rinsed in 100% ETOH followed by 100% methylmethacrylate for 4 h under vacuum at 20 in Hg, then embedded in methacrylate. Longitudinal sections of 70 μm thickness were cut in ulna using a diamond wire saw (DDK, Delaware Diamond Knives, Wilmington, DE).

Microdamage measurement

The sections were examined microscopically to identify regions with accumulation of tracer in PET images in order to verify microdamaged regions histologically. All measurements were performed by one histomorphometrist, blinded to group affiliation, using a semi-automatic digitizing system (Bioquant System IV) attached to a Nikon Optiphot equipped with brightfield sources. Stained microcracks were identified by their shape, some depth of field and permeation of stain into the crack walls [6]. Crack number and total crack length (μm) were measured under ×120 magnifications.

Experimental design

In order to determine the sensitivity and specificity of high-resolution PET imaging of bone microdamage in vivo, 3 experiments were carried out. The rat axial ulnar loading model was used to produce microdamage in bone under well-controlled loading conditions [2,24].

Experiment 1: detection of the bone microdamage using high-resolution PET in vivo

Before fatigue loading, background PET scanning was carried out in all the animals ($n = 5$; Table 1). The right ulnae of the rats were then loaded with a peak load of 17 N at 2 Hz, as described below. Loading was stopped when stiffness loss reached 20%. Eleven days later, the left ulnae of the animals were loaded in the same manner as the right ones. One day after the left ulnae were loaded (12 days after the right ulnae were loaded), the PET scanning was performed again in those animals.

Experiment 2: registering the high-resolution PET image of microdamage with autoradiography and histological analysis

Four female SD rats were used to compare in vivo PET images with in vitro autoradiographic images. The right ulnae of the rats were loaded with a peak load of 17 N at 2 Hz. Loading was stopped when stiffness loss reached 20% (about 6000–7000 cycles). Immediately after PET scanning, animals were sacrificed, and ulnae were dissected. Ulnae were embedded in wax, and 200-μm longitudinal sections were cut. The sections were exposed to a Fuji phosphor storage plate in a cassette for 20 min. The film was scanned using FUJI FLA-2000 Fluorescence and Stored Phosphor Imaging System (Fuji Medical System, USA) coupled with a Macintosh computer to produce a digital image representing the quantity of [F-18] in the tissue section. The distribution of radioactivity along longitudinal section of ulna was used to compare with in vivo PET images and histological findings. After autoradiography, those sections were mounted on slides and examined under the microscope.

Experiment 3: specificity of high-resolution PET imaging of bone microdamage in vivo

The right ulnae of six rats (body weight: about 280 g) were cyclically loaded to 20% stiffness loss (4000–8000 cycles), whereas the left ulnae were loaded on the same day with half of the loading cycles (2000–4000 cycles) used on the right sides. PET imaging was performed on the following day.

Data analysis

The data are expressed as mean ± SEM (standard error of the mean). Differences among group means were tested for significance by analysis of

Table 1
Schedule for PET imaging

Day 1	Day 2	...	Day 13	Day 14
1st PET scanning (background)	Fatigue loading of right ulnae		Fatigue loading of left ulnae	2nd PET scanning

variance (ANOVA), followed by Fisher's protected least significant difference (PLSD) for all the comparisons.

Results

The activity of all the animals was not affected by fatigue loading based on the observations following mechanical loading. Fatigue loading induced bone damage at the midshaft of the rat ulna. This was observed as a 20% loss of stiffness and detected histologically by en bloc basic fuchsin staining. In this study, fatigue loading produced 1–2 microcracks with a total crack length about 1300–2000 μm at the midshaft of the longitudinal sections of ulnae. Resorption spaces can be observed 12 days after cyclic loading.

Experiment 1: detection of the bone microdamage using high-resolution PET in vivo

The background PET scanning showed that there was minimal tracer accumulation in the midshaft of either right or left ulna before loading. Accumulation of tracer was seen at the ulnar midshaft 1 day following loading (left ulna) and was enhanced 12 days following the cyclic load application (right ulna) (Fig. 1). The PET image intensity 1 day as well as 12 days following fatigue loading increased significantly ($P < 0.001$ and $P < 0.001$) compared with the background intensity at the midshaft of ulna (Fig. 2). Comparing basic fuchsin stained longitudinal histological sections (Fig. 3) microscopically with the PET images, we found a 1–2 mm range of microdamage located about 13 mm from the distal end of the ulna, consistent with the tracer accumulation area in the midshaft of the ulna using PET scanning. Where there was no increase in tracer accumulation in PET images, no microdamage was found microscopically. Collectively, these data show that high-resolution PET can detect newly created microdamage within 1 day in vivo, and that microdamage detected in this way is co-localized with damage detected by histological procedures.

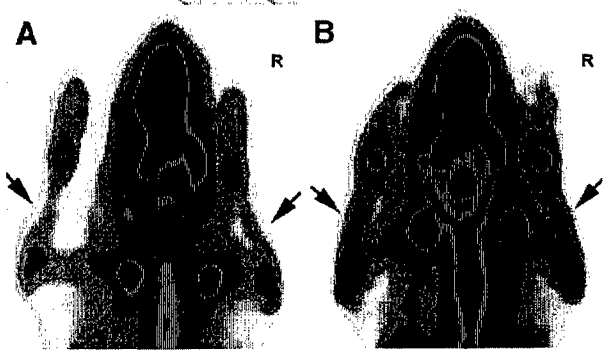

Fig. 1. The images of PET scanning before (A) and after (B) fatigue loading. The intensity of the "hot spot" in the right ulna in panel B (loaded 12 days before imaging) was higher than the intensity of the left ulna in panel B (loaded 1 day before imaging).

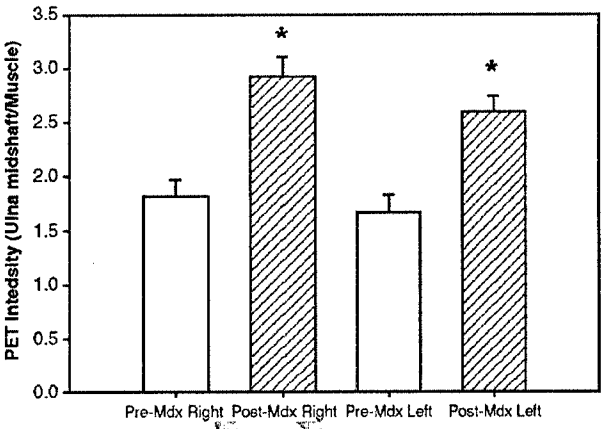

Fig. 2. PET imaging intensity was calculated from coronal maximum intensity projection images. The figure shows intensity, normalized by the intensity of forearm muscle, of the left ulna and the right ulna before loading (white bars) and after loading (line bars). A significant increase in intensity at midshaft of both left and right ulnae could be seen in the loaded ulnae ($P < 0.001$). The intensity at the right was slightly higher than that at the left.

Experiment 2: registering the high-resolution PET image of microdamage with autoradiography and histological analysis

The PET image showed a "hot spot" about 13 mm from the wrist joint (Fig. 4). At the same distance from the wrist, we found an enhanced accumulation of radioactive tracer by autoradiography and were able to observe a crack histologically. These data confirm that high-resolution PET imaging corresponds to regions of microdamage confirmed by more established autoradiographic and histological techniques.

Experiment 3: specificity of high-resolution PET imaging of bone microdamage in vivo

There was no enhancement of tracer accumulation on the left ulnae, which was loaded to levels that did not create damage or

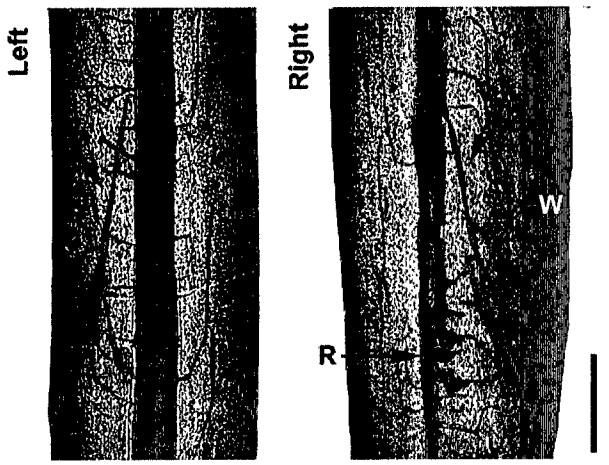

Fig. 3. Microcracks induced by fatigue loading were found in the "hot spot" areas of both left and right ulnae, stained by en bloc Basic fuchsin. Left ulna: only microcracks were found 1 day after fatigue loading. Right ulna: besides microcracks, woven bone (W) on the periosteal surface and resorption spaces (R) in the cortex were found 14 days after loading. Scale bar = 500 μm.

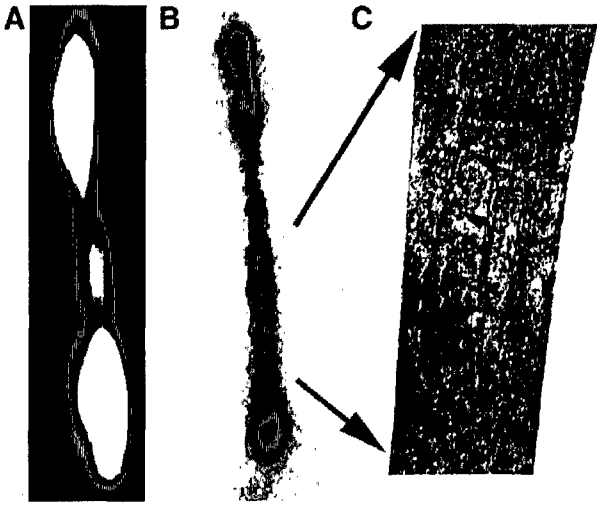

Fig. 4. A "hot spot" was seen in vivo at the ulnar midshaft with PET imaging (A) at 13-mm distance from the wrist joint. At the same place, the in vitro autoradiography (B) showed the enhanced accumulation of radioactive tracer and the examination under microscope (C) disclosed a microcrack (arrows) in the longitudinal section.

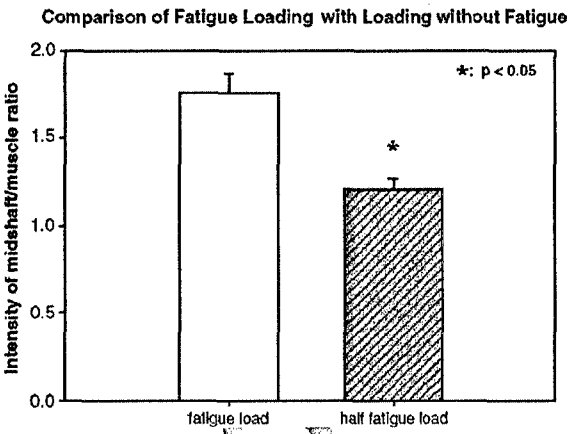

Fig. 6. PET imaging intensity was significantly higher at the midshaft of ulnae with microdamage induced by fatigue loading than the midshaft of ulnae loaded but without microdamage.

fatigue (Fig. 5); the absence of damage was confirmed histologically. Enhanced accumulation of tracer was observed only on the right ulnae, which were fatigue loaded to a 20% stiffness loss; this was also consistent with the presence of histologically detectable microdamage on these ulnae. Compared with the non-fatigued ulnae, the high-resolution PET image intensity at midshaft of ulnae was significantly ($P < 0.05$) increased by the induction of microdamage caused by fatigue loading (Fig. 6).

Discussion

The data in the present study show [1] [^{18}F] NaF PET can image areas of bone microdamage in vivo even within 1 day after the damage is created [2]; the PET image is even more intense after initiation of intracortical remodeling (repairing of microdamage) [3]; areas of enhanced [^{18}F] NaF tracer uptake were specific to the microdamage areas. These data suggest that PET scanning is sensitive to the newly created microdamage as well as specific to the microdamage area.

In the present study, we successfully reproduced the rat ulnar fatigue loading model which has previously been used to study the bone microdamage in vivo [2,23]. Axial end-load bending of rat ulnae results in bone strains distributed in the ulnar diaphysis as tension on the medial ulnar surface and compression on the lateral ulnar surface. Our data showed that bone damage occurred on the tension side of the cross-section of the ulna. The bone microdamage induced in our loading system histologically resembles that reported previously [2,23]. Twelve days after bone fatigue, resorption spaces were observed. Because rats do not under normal conditions have osteonal remodeling, this model allows us the potential to detect and evaluate regions of increased bone metabolism without the overlying confounding effects of cortical bone turnover.

Imaging bone microdamage in vivo has been a challenge because of the small size of the cracks (~60 μm long × <1 μm wide in cross-section). At present, computed tomography (CT) and magnetic resonance imaging (MRI) do not have sufficient resolution to directly image bone microdamage in vivo. PET imaging has been used to look for bone tumors and metastases. Previous studies have shown that Na^{18}F PET is more sensitive to bone metastases than planar bone scintigraphy and F-18

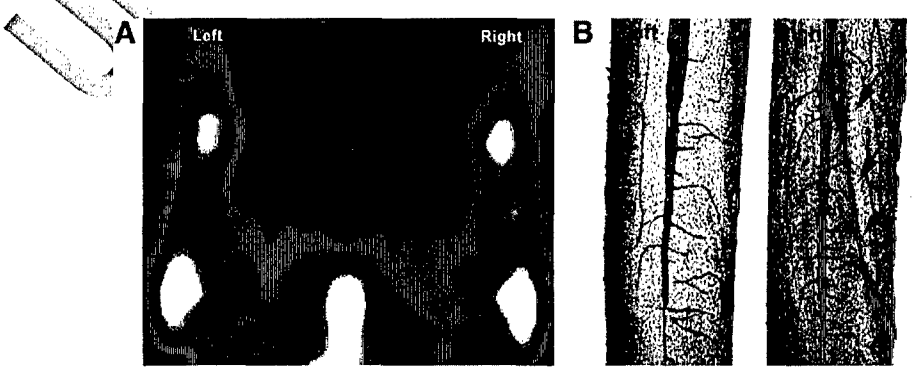

Fig. 5. Enhanced accumulation of tracer was only seen on the right ulnae (fatigue loading sides), but not on the left ulnae (loaded without fatigue), which was consistent with the microcracks seen under microscope.

fluorodeoxyglucose (FDG)-PET [8]. The data in our study suggest that high-resolution $Na^{18}F$ PET is also useful to detect bone microdamage in vivo.

In the present study, $Na^{18}F$ PET detects the newly created microdamage 1 day after fatigue loading. Compared with other bone-seeking radiopharmaceuticals such as ^{99m}Tc-labeled diphosphonates (anionic complexes), [^{18}F]fluoride ion is small and is naturally incorporated into the bone matrix. [^{18}F]fluoride ion exchange with hydroxyl groups in the hydroxyapatite crystal of bone to form fluoroapatite. [^{18}F]fluoride is deposited preferentially at the surface of bone, where remodeling or turnover is greatest [14]. Bone microdamage opens more bone surface for the [^{18}F]fluoride ion to incorporate into bone tissue than in undamaged bone. Bone remodeling is not activated within 1–2 days of production of microdamage, but the increased bone surface allows more [^{18}F]fluoride ion to exchange with hydroxyl groups in the hydroxyapatite crystal of bone and allows visualization This suggests that $Na^{18}F$ PET imaging is sensitive to detect bone microdamage in vivo.

PET intensity increased 12 days after loading compared to the intensity of newly created microdamage in vivo. This is caused by the activation of intracortical remodeling that begins 7–10 days after fatigue loading, which produces more bone surface in the damaged bone location. Also, there is woven bone formation at the periosteal surface of ulna at this time, which leads to greater uptake of $Na^{18}F$.

The specificity of PET imaging of bone microdamage probably is not related to bone metabolism, at least for the newly created microdamage. Skeletal uptake of bone-seeking radiopharmaceuticals such as ^{99m}Tc-labeled diphosphonates and [^{18}F]fluoride is influenced by several factors: metabolic activity of the bone tissue, bone blood flow, molecular size, net electric charge of the molecule, capillary surface, capillary permeability and local pH [18]. Mechanical loading can increase bone blood supply and interstitial fluid flow in bone [10,17] as well as activate osteoblast differentiation and proliferation [22]. Both factors increase accumulation of radioactive tracer in bone. However, in our study, enhanced accumulation of tracer was only seen on the loaded ulnae with microdamage, not on the loaded ulnae in which bone formation was initiated but microdamage was not produced. This implies that PET can distinguish the increased blood flow associated with mechanically adaptive modeling and remodeling from the $Na^{18}F$ accumulation relating specifically to mechanically induced microdamage in the early stage of production of microdamage. These data suggest that $Na^{18}F$ PET imaging detects bone microdamage, and not just local blood flow, in vivo.

PET intensity can be used to estimate the activities of osteoblasts and osteoclasts. In $Na^{18}F$ PET scanning, the activities of osteoblasts and osteoclasts are believed to determine the amount of [^{18}F]fluoride chemisorption and incorporation into the bone matrix. It is known that both osteoclasts and osteoblast play important roles in the repair of bone microdamage [13]. Our data show there is a time-course curve in PET intensity following the production of microdamage, suggesting that changes of intensity may reflect the time-course of bone repair. This remained to be investigated in the future.

In conclusion, the data in our study indicated that PET scanning is both sensitive and specific to the newly created microdamage. It can distinguish between the effects of mechanical loading that does not produce damage and fatigue loading that creates damage. High-resolution $Na^{18}F$ PET shows promise as a non-invasive means to image bone microdamage.

Acknowledgments

The authors would like to thank Bruce Mock and the PET chemistry group for the production of NaF, and Tanya Martinez, K. Lee Stone and Terry Mcbride for their assistance with the collection of imaging data. We also thank Keith W. Condon for his assistance with tissue processing. This work was supported in part by the Indiana Genomics Initiative. The Indiana Genomics Initiative is supported in part by the Lilly Endowment. The work was also supported in part by U. S. Army Research and Material Command (UAMRMC #03351012).

References

[1] Bennell KL, Hart P, Nattrass C, Wark JD. Acute and subacute changes in the ultrasound measurements of the calcaneus following intense exercise. Calcif Tissue Int 1998;63:505–9.

[2] Bentolila V, Boyce TM, Fyhrie DP, Drumb R, Skerry TM, Schaffler MB. Intracortical remodeling in adult rat long bone after fatigue loading. Bone 1998;23:275–81.

[3] Berding G, Burchert W, van den Hoff J, Pytlik C, Neukam FW, Meyer GJ, et al. Evaluation of the incorporation of bone grafts used in maxillofacial surgery with [18F]fluoride ion and dynamic positron emission tomography. Eur J Nucl Med 1995;22:1133–40.

[4] Burr DB. Microdamage in bone. Curr Opin Orthop 1997;8:8–14.

[5] Burr DB, Forwood MR, Fyhrie DP, Martin RB, Shaffler MB, Turner CH. Bone microdamage and skeletal fragility in osteoporotic and stress fracture. J Bone Miner Res 1997;12:6–15.

[6] Burr DB, Hooser M. Alterations to the en bloc basic fuchsin staining protocol for the demonstration of microdamage produced in vivo. Bone 1995;17:431–3.

[7] Burr DB, Stafford T. Validity of the bulk-staining technique to separate artifactual from in vivo bone microdamage. Clin Orthop 1990:305–8.

[8] Cook GJ, Houston S, Rubens R, Maisey MN, Fogelman I. Detection of bone metastases in breast cancer by 18FDG PET: differing metabolic activity in osteoblastic and osteolytic lesions. J Clin Oncol 1998;16:3375–9.

[9] D'Ambrosia RD, Riggins RS, DeNardo SJ, DeNardo GL. Fluoride-18 scintigraphy in avascular necrotic disorders of bone. Clin Orthop 1975:146–55.

[10] Hillsley MV, Frangos JA. Bone tissue engineering: the role of interstitial fluid flow. Biotechnol Bioeng 1994;43:573–81.

[11] Hoh CK, Hawkins RA, Dahlbom M, Glaspy JA, Seeger LL, Choi Y, et al. Whole body skeletal imaging with [18F]fluoride ion and PET. J Comput Assist Tomogr 1993;17:34–41.

[12] Lee TC, Arthur TL, Gibson LJ, Hayes WC. Sequential labelling of microdamage in bone using chelating agents. J Orthop Res 2000;18:322–5.

[13] Mori S, Burr DB. Increased intracortical remodeling following fatigue damage. Bone 1993;14:103–9.

[14] Narita N, Kato K, Nakagaki H, Ohno N, Kameyama Y, Weatherell JA. Distribution of fluoride concentration in the rat's bone. Calcif Tissue Int 1990;46:200–4.

[15] Nicholson PH, Bouxsein ML. Quantitative ultrasound does not reflect mechanically induced damage in human cancellous bone. J Bone Miner Res 2000;15:2467–72.

[16] Petren-Mallmin M. Clinical and experimental imaging of breast cancer metastases in the spine. Acta Radiol, Suppl 1994;391:1–23.

[17] Piekarski K, Munro M. Transport mechanism operating between blood supply and osteocytes in long bones. Nature 1977;269:80–2.
[18] Piert M, Zittel TT, Becker GA, Jahn M, Stahlschmidt A, Maier G, et al. Assessment of porcine bone metabolism by dynamic. J Nucl Med 2001;42: 1091–100.
[19] Rouze NC, Hutchins GD. Design and characterization of IndyPET-II: a high-resolution, high-sensitivity dedicated research scanner. IEEE Trans Nucl Sci 2003;50:1491–7.
[20] Schaffler MB, Pitchford WC, Choi K, Riddle JM. Examination of compact bone microdamage using back-scattered electron microscopy. Bone 1994; 15:483–8.
[21] Schiepers C, Hoh CK. Positron emission tomography as a diagnostic tool in oncology. Eur Radiol 1998;8:1481–94.
[22] Turner CH, Owan I, Alvey T, Hulman J, Hock JM. Recruitment and proliferative responses of osteoblasts after mechanical loading in vivo determined using sustained-release bromodeoxyuridine. Bone 1998;22: 463–9.
[23] Verborgt O, Gibson GJ, Schaffler MB. Loss of osteocyte integrity in association with microdamage and bone remodeling after fatigue in vivo. J Bone Miner Res 2000;15:60–7.
[24] Verborgt O, Tatton NA, Majeska RJ, Schaffler MB. Spatial distribution of Bax and Bcl-2 in osteocytes after bone fatigue: complementary roles in bone remodeling regulation? J Bone Miner Res 2002;17:907–14.
[25] Villanueva AR, Longo III JA, Weiner G. Staining and histomorphometry of microcracks in the human femoral head. Biotech Histochem 1994;69:81–8.
[26] Zioupos P, Currey JD, Mirza MS, Barton DC. Experimentally determined microcracking around a circular hole in a flat plate of bone: comparison with predicted stresses. Philos Trans R Soc Lond, B Biol Sci 1995;347: 383–96.

Vol. 20, No. 5
May 2005
pp. 717–894

Celebrating 20 years of advancing science

JBMR

CLINICAL

Men with low skeletal muscle mass had narrower bones, thinner cortices, and decreased bending strength, as well as impaired balance and increased falls risk

TRANSLATIONAL

Mechanical loading of rat ulna increased structural properties 2-fold but fatigue resistance 100-fold, supporting the value of moderate exercise

BASIC

Ectopic bone formation by human bone marrow stromal cells was promoted more efficiently by sustained presentation of BMP-4 and VEGF together

ASBMR

Published monthly by
The American Society for Bone and Mineral Research

JOURNAL OF BONE AND MINERAL RESEARCH
Volume 20, Number 5, 2005
Published online on December 20, 2004; doi: 10.1359/JBMR.041222

Bone Adaptation to a Mechanical Loading Program Significantly Increases Skeletal Fatigue Resistance

Stuart J Warden,[1,2] Julie A Hurst,[3] Megan S Sanders,[2] Charles H Turner,[2,4] David B Burr,[3,4] and Jiliang Li[3]

ABSTRACT: Using a mechanical loading program to induce bone adaptation, we found that small (<2-fold) changes in the structural properties of the rat ulna increased its fatigue resistance >100-fold. This indicates that a moderate exercise program may be an effective preventative strategy for stress fractures.

Introduction: There are currently limited preventative strategies for stress fractures. Because stress fracture risk is directly influenced by skeletal properties, it has been hypothesized that modification of these properties using a mechanical loading program may positively influence risk. The aim of this study was to investigate whether the bone changes associated with a mechanical loading program can enhance skeletal fatigue resistance.
Materials and Methods: Site-specific mechanical loading was performed on one forearm of adult female Sprague-Dawley rats using the axial compression loading model. Loading was performed 3 days/week for 5 consecutive weeks to induce adaptation. The loaded and nonloaded ulnas in each animal were removed after the loading program, and their material and structural properties were determined. The ulna pairs were subsequently loaded until fatigue failure at the same constant peak axial load.
Results: Mechanical loading induced consistent and predictable changes in the structural properties of loaded ulnas, with the largest change being a nearly 2-fold increase in midshaft minimum second moment of area (I_{MIN}). The mechanical-loading induced bone changes resulted in a >100-fold increase in fatigue resistance in loaded ulnas, with resistance being exponentially related to the structural properties of the ulna.
Conclusions: This study found that by enhancing the structural properties of a bone through a mechanical loading program, its fatigue resistance could be significantly improved. This indicates that an exercise program aimed at modifying bone structure may be used as a possible prevention strategy for stress fractures.
J Bone Miner Res 2005;20:809–816. Published online on December 20, 2004; doi: 10.1359/JBMR.041222

Key words: adaptation, biomechanics, exercise, mechanical loading, stress fractures

INTRODUCTION

A MAJOR ROLE OF THE SKELETON is to provide internal support to enable the force of gravity to be countered. In fulfilling this role, bones are exposed to repetitive bouts of mechanical loading. As with other structural materials, a natural phenomenon associated with repetitive loading of bone is the generation of damage (often termed microdamage).[1–3] Although bone is unique from nonbiological materials in that it is capable of self-repair of damage through targeted and nontargeted remodeling,[4] imbalances can develop between damage generation and removal. The subsequent accumulation of damage is believed to contribute to the development of stress fracture.[1,5]

A stress fracture represents the inability of a bone to withstand repetitive bouts of mechanical loading, which results in structural fatigue (fatigue failure) and the resultant signs and symptoms of localized pain and tenderness. They are particularly common among athletes and military recruits[6] and have significant ramifications in terms of morbidity and time lost from participation. Despite their clinical significance, there are currently limited preventative strategies for stress fractures.[7] This primarily results from their relatively unknown etiology, which is considered to be multifactorial involving a combination of extrinsic and intrinsic factors.[8] Extrinsic factors refer to features of the loading environment (such as training program design, equipment and surfaces), whereas intrinsic factors refer to characteristics within individual's themselves. The latter are the focus of this study and include skeletal properties such as BMD (material properties) and the distribution of this bone (structural properties).

The contribution of skeletal properties to the ability of a bone to withstand repetitive low-magnitude loads is estab-

The authors have no conflict of interest.

[1]Department of Physical Therapy, School of Health and Rehabilitation Sciences, Indiana University, Indianapolis, Indiana, USA; [2]Department of Orthopaedic Surgery, Indiana University School of Medicine, Indianapolis, Indiana, USA; [3]Department of Anatomy and Cell Biology, Indiana University School of Medicine, Indianapolis, Indiana, USA; [4]Biomechanics and Biomaterials Research Center, Indiana University School of Medicine, Indianapolis, Indiana, USA.

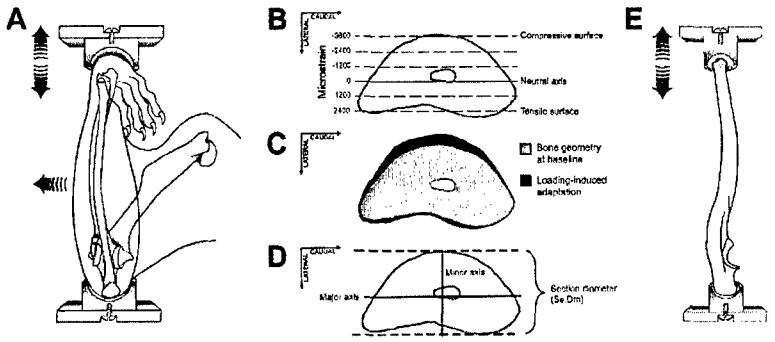

FIG. 1. The rat ulna axial loading model. (A) Schematic diagram of the loading model. The right distal forelimb is fixed between upper and lower cups (shown in hemisection) on a loading system. When force is applied to one of the cups, the pre-existing mediolateral curvature of the ulnar diaphysis becomes accentuated and translates most (80%)[30] of the axial load into a bending moment. (B) The bending of the ulna under axial compression generates medial surface compression and lateral surface tension at the midshaft (shown in cross-section), with the ratio of compressive to tensile strain being 1.53.[30] There is no strain along the axis through which the bone is bending (neutral axis). (C) The loading pattern causes new bone to be formed on surfaces of high strain (medial and lateral surfaces), with the amount of new bone formed being related to the strain magnitude on the respective surface (i.e., more bone is formed on the medial surface than lateral surface). There is minimal new bone formation near the neutral axis (caudal and cranial surfaces) where there is least microstrain during loading. (D) As the medio-lateral plane in the rat ulna corresponds with its minor axis (plane of least bending rigidity), with the minimum second moment of area (I_{MIN}) occurring along that axis, bone adaptation in this model predominantly causes an increase in I_{MIN}. There is minimal change in the maximum second moment of area (I_{MAX}) because this corresponds with the major axis (the plane of greatest bending), which is located in the cranio-caudal plane. The section diameter (Se.Dm) of the ulna is measured as its largest diameter in the plane parallel to the I_{MIN} axis. (E) Fatigue testing of rat ulnas in axial compression. After death, the ulnas are dissected free and mounted in a similar rig as used for in vivo loading (but with smaller cup sizes). The bones are cyclically loaded in axial compression until fatigue failure (fracture). Modified from Robling et al.[29] and Warden et al.[27]

lished. Seminal work by Carter and Hayes[9,10] showed that both the material and structural properties of bone directly influence its fatigue properties. While these findings have gained variable clinical support from numerous cross-sectional studies,[11–17] statistically more powerful prospective studies have shown that stress fracture susceptibility is directly related to the structural properties of the skeleton.[18–21] Individuals with lower bone mass and smaller bones are at greater risk of stress fracture than those with higher bone mass and larger bones.[18–21]

Because stress fracture risk is directly influenced by skeletal properties, it has been hypothesized that modification of these properties through the exploitation of the adaptive ability of bone may be used as a means of influencing an individual's risk.[18,22–24] One method of achieving this is to use a mechanical loading program. While repetitive mechanical loading can lead to skeletal fatigue, it can also act as a potent anabolic stimulus.[25] Bone is inherently mechanosensitive and responds and adapts to its mechanical environment.[26,27] An exercise program that alters the material and structural properties of the skeleton may be an effective means of modifying an individual's risk for stress fracture. However, there is currently no direct evidence supporting this hypothesis. The aim of this study was to investigate whether the bone changes associated with a mechanical loading program can enhance skeletal fatigue resistance.

MATERIALS AND METHODS

Animals

Twenty-four adult virgin female Sprague-Dawley rats (weight, 280–300 g; age, 18–20 weeks) were purchased from Harlan Sprague-Dawley (Indianapolis, IN, USA) and acclimated for 1 week before experimentation. Animals had ad libitum access to standard rat chow and water at all times, and all procedures were performed in accordance with the guidelines of the Institutional Animal Care and Use Committee of Indiana University.

Mechanical loading

Site-specific mechanical loading was achieved using the rat ulna axial loading model (Fig. 1A).[28] In this model, the right forearm of each animal was axially loaded across the olecranon and flexed carpus, with the animal under isoflurane anesthesia (Abbott Laboratories, North Chicago, IL, USA). The ulna is the major load-bearing bone in this model, carrying two-thirds of the applied load, with the remaining load being borne by the radius.[31] The load on the ulna is translated mostly into a bending moment that accentuates the bone's mediolateral curvature. This results in compressive strain on the medial surface and tensile strain on the lateral surface (Fig. 1B). This strain distribution is similar to that resulting from normal limb usage during locomotion in rats[32] and results in strain magnitude-related bone adaptation on the medial and lateral surfaces of the ulna (Fig. 1C). Because the medio-lateral plane in the rat ulna corresponds with the minimum second moment of area (I_{MIN}), bone adaptation in this model predominantly causes an increase in I_{MIN} (Fig. 1D).

Loading was introduced using an electromechanical actuator and applied using a 2-Hz haversian waveform for 360 cycles/day, 3 days/week for 5 consecutive weeks. The peak load magnitude was 17N, which elicits a compressive strain of ~3600 $\mu\varepsilon$ on the medial surface of the ulna midshaft.[30] Left ulnas served as internal controls and were not loaded.

Normal cage activity was allowed between loading sessions. Animals were killed 5 weeks after the final loading session, and the right and left ulnas were dissected free and stored in 70% alcohol. Short-term storage in 70% alcohol has been shown to have no negative effects on the mechanical properties of bone.[33]

Assessment of bone adaptation

Adaptation to mechanical loading was determined by assessing both the right and left ulnas from each animal using DXA, pQCT, and μCT. DXA was performed using a PIXImus II mouse densitometer (Lunar Corp., Madison, WI, USA) with ultra-high resolution (0.18 × 0.18 mm/pixel). Scanning was performed with each ulna positioned on its lateral side, and the left and right ulna from each individual animal was scanned side-by-side on the same scan. On completion of each scan, mutually exclusive region of interest boxes were drawn around each ulna from which whole ulna BMC (mg) and areal BMD (aBMD; g/cm^2) were collected. aBMD is a structural bone property because it is derived from the areal projection of a bone and is, therefore, dependent on bone size.

pQCT was performed using a Norland Stratec XCT Research SA+ pQCT (Stratec Electronics, Pforzheim, Germany). Each ulna was placed in a plastic tube filled with 70% ethanol and centered in the gantry of the machine. After the performance of a scout view to enable scan localization, a cross-sectional scan was performed at the ulna midshaft using a 0.46-mm collimation and 70-μm voxel size. Analyses were restricted to cortical bone, because trabecular bone is not normally present at the ulna midshaft. The bone edge was detected using contour mode 1 with a threshold of 400 mg/cm^3 within the Stratec software. BMC (mg/cm) and volumetric BMD (vBMD; mg/cm) were recorded for each bone. vBMD is a material bone property because it describes the amount of mineral present, independent of bone size.

μCT was performed using a desktop μCT machine (μCT-20; Scanco Medical AG, Auenring, Switzerland). Each ulna was placed in a plastic tube filled with 70% ethanol and centered in the gantry of the machine. A scout scan was performed, and a cross-sectional scan was performed at the ulna midshaft using a 7-μm voxel size. Each scanned image was imported into Scion Image v4.0.2 for Windows (Scion Corp., Fredrick, MD, USA), wherein the structural properties of cortical area (Ct.Ar; mm^2), and the maximum (I_{MAX}; mm^4) and minimum (I_{MIN}; mm^4) second moments of area were determined using standard and customized macros. In addition, the section diameter (Se.Dm; mm) was determined as the largest diameter of the bone in the plane parallel to the I_{MIN} axis (Fig. 1D).

Determination of strain during fatigue testing

To permit the calculation of microstrain during fatigue testing, right (loaded) and left (nonloaded) ulnas from four animals were chosen at random for a preliminary load-strain calibration experiment. The ulnas were rehydrated and brought to room temperature overnight in a saline bath. A single element strain gauge (EA-06-015DJ-120; Measurements Group, Raleigh, NC, USA) was bonded with cyanoacrylate (M-Bond 200; Measurements Group) at the midpoint of each ulna. The ulnas were axially loaded at four different peak loads (with a 0.05N preload) using the loading system to be used for fatigue testing (see below). The strain gauge voltage signal was routed through a signal conditioning amplifier (Model 2210; Measurements Group), and the peak-to-peak voltage was measured on a digital oscilloscope. Voltage was converted to strain using a calibration factor derived from measured and calculated (using beam theory) strains collected using an aluminum cantilever. A graph was constructed plotting με/N versus c/I_{MIN}, where c is 2/3 of the Se.Dm. A value of 2/3 of the Se.Dm is used because this best represents the ratio of bending to compression at the ulna midshaft in the rat ulna axial compression model.[30] The slope of the graph (0.018 με/N/mm^{-3}) matched that obtained in previous work[34] and represents average ulna compliance (strain per given load). This slope was used to predict strain or load during fatigue testing in experimental ulnas. Strain or load in the experimental ulnas was estimated from their I_{MIN} and c, along with the data obtained from the strain gauged ulnas, using the equation:

$$\frac{\mu\varepsilon}{N} = \frac{c}{0.018 \times I_{MIN}}$$

Fatigue testing

The remaining ulna pairs were randomly divided into two groups: (1) same load group (N = 10) and (2) same strain group (N = 10). In the same load group, the right (loaded) and left (nonloaded) ulna pairs were loaded at a constant peak axial load of 25N until fatigue failure, whereas those in the same strain group were loaded at an initial peak strain of 5000 με until fatigue failure. Fatigue failure was defined as occurring when the bone failed completely and could no longer withstand the applied load. Ulnas were fatigued ex vivo to permit strict control over loading variables, with ex vivo axial loading of the ulna generating the same strain pattern as occurs with its in vivo loading.[31] The load in the same load group was chosen to ensure that these specimens would break within 1–2 × 10^6 cycles, a practical limit. For testing, ulnas were rehydrated and brought to room temperature overnight in a saline bath, fixed with 0.5N of preload between two opposing cup-shaped platens on an electromagnetic actuator (Bose ElectroForce 3200 series; EnduraTEC, Minnetonka, MN, USA), and axially loaded in load control until fatigue failure (fracture; Fig. 1E). Loading was performed continuously in a room temperature (20°C) saline bath using a 5-Hz haversian waveform. The number of cycles until fatigue failure was recorded for each bone.

Statistical analyses

Statistical analyses were performed with the Statistical Package for Social Sciences (SPPS 6.1.1; Norusis/SPSS, Chicago, IL, USA) software, with a level of significance set at 0.05 for all tests. Bone material, structural, and fatigue properties were compared between loaded and nonloaded ulnas using paired t-tests. The relationship between the ma-

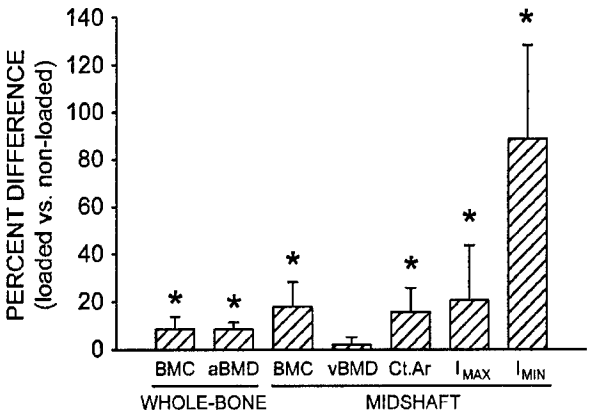

FIG. 2. Bone adaptation in response to the mechanical loading program. Bars represent the mean percent difference between the loaded and nonloaded ulnas for all animals (N = 24). *Significantly different from 0% (no difference between loaded and nonloaded ulnas; $p < 0.01$, single sample t-test with population mean of 0%). Error bars represent ± SD.

terial and structural properties of each ulna in the same load group and fatigue resistance was determined using the Spearman rank correlation coefficient.

RESULTS

Mechanical loading increased local skeletal structural properties

Axial loading of the forelimb three times per week for 5 weeks induced consistent changes in the structural properties of the loaded ulnas (Fig. 2; Table 1). The largest effect was on I_{MIN}, which was 86.9% larger in loaded ulnas than contralateral nonloaded ulnas. BMC and aBMD for the entire ulna were increased, as was BMC for the ulna midshaft. However, vBMD of the ulnar midshaft was unchanged (Table 1), indicating that loading did not significantly change the material properties of the ulna.

Mechanical loading-induced bone changes increased fatigue resistance by >100-fold

The mechanical loading-induced bone changes resulted in a significant increase in ulna fatigue resistance. Ulnas failed in fatigue typically with a comminuted fracture with a medial (compression) butterfly fragment. When fatigued at 25N, loaded ulnas took 107 times more cycles before fatigue failure than nonloaded ulnas, with fatigue failure occurring in loaded ulnas after 1.58 ± 1.01 million cycles compared with the 14,572 ± 19,243 cycles required in nonloaded ulnas (Fig. 3). Because these ulna pairs were exposed to the same load (25N), they experienced significantly different magnitudes of microstrain. Nonloaded ulnas experienced 5361 ± 618 με compared with the 3683 ± 370 με experienced by loaded ulnas ($p < 0.001$), indicating that the 5-week loading regimen reduced ulna bone strain by ~30%. When the peak microstrain levels were equalized for the fatigue test (same strain group), there was no significant difference in cycles to fatigue failure (p = 0.65; Fig. 3), indicating that there was

TABLE 1. LOADING-INDUCED CHANGES IN ULNA PROPERTIES*

	Nonloaded	*Loaded*
Whole bone		
BMC (mg)†	100.7 ± 5.5	108.7 ± 5.3¶
aBMD (mg/cm²)†	100.7 ± 1.7	108.9 ± 3.2**
Midshaft		
BMC (mg/mm)‡	2.97 ± 0.27	3.52 ± 0.27**
vBMD (mg/cm)‡	1207.3 ± 33.8	1228.0 ± 26.8††
Ct.Ar (mm²)§	2.16 ± 0.10	2.64 ± 0.16**
I_{MAX} (mm⁴)§	0.91 ± 0.10	1.04 ± 0.12¶
I_{MIN} (mm⁴)§	0.18 ± 0.02	0.33 ± 0.06**

* Values are mean ± SD.
† Assessed using DXA.
‡ Assessed using pQCT.
§ Assessed using μCT.
Significance of nonloaded vs. loaded comparison (paired t-test) indicated as follows: ¶$p < 0.05$; **$p < 0.01$; ††$p > 0.05$.

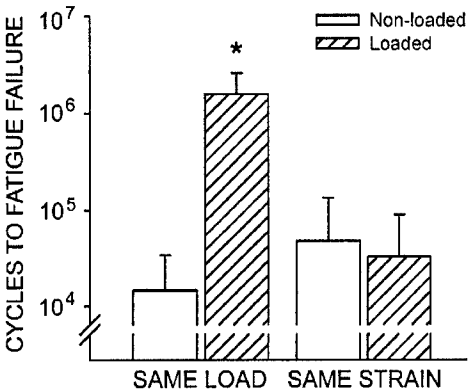

FIG. 3. Effect of bone adaptation on skeletal fatigue resistance. Cycles to fatigue failure is plotted on a log scale. *Significantly different from nonloaded ($p < 0.001$, paired t-test). Error bars represent ± SD.

no substantial difference in the material properties of the loaded and nonloaded ulnas. Ulnas in this group were exposed to different load magnitudes to generate the desired level of microstrain (5000 με), with nonloaded ulnas requiring 21.9 ± 1.7N compared with the 33.6 ± 4.9N required in loaded ulnas ($p < 0.001$).

Fatigue resistance was exponentially related to bone structural properties

The relationship between fatigue resistance and the material and structural properties of each ulna was explored for the same load group. A consistent positive exponential relationship existed between each bone measurement and the number of loading cycles until fatigue failure (Figs. 4A–4G). All correlations were significant except for vBMD (r = 0.432, p = 0.06; Fig. 4D), indicating that bone material properties had little correlation with its fatigue resistance. The best correlation to cycles to fatigue failure was I_{MIN} (r = 0.871, $p < 0.001$; Fig. 4G). Variance in I_{MIN} could explain 75.9% of the variance in cycles to failure. Because bone structural properties influence microstrain during loading,

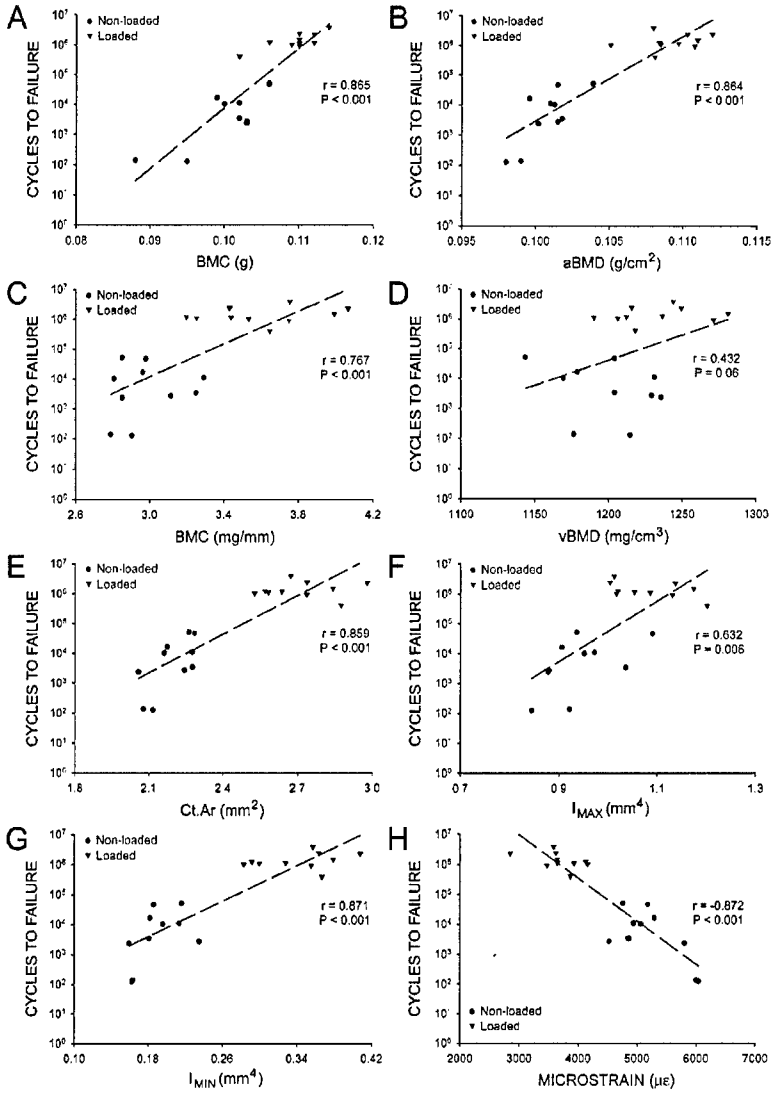

FIG. 4. Relationship of skeletal fatigue resistance to (A) whole bone BMC, (B) whole bone aBMD, (C) midshaft BMC, (D) midshaft vBMD, (E) midshaft Ct.Ar, (F) midshaft I_{MAX}, (G) midshaft I_{MIN}, and (H) microstrain. Cycles to failure is plotted on a log scale.

fatigue resistance was significantly negatively correlated with microstrain ($r = -0.872$; $p < 0.001$) such that increasing microstrain decreased fatigue resistance (Fig. 4H).

DISCUSSION

This study found that by enhancing the structural properties of a bone through a mechanical loading program, its fatigue resistance could be significantly improved. Mechanical loading induced predictable and consistent changes in the structural properties of the rat ulna, with the largest assessed change being a nearly 2-fold increase in midshaft I_{MIN}. The relatively small loading-induced change in the bone structure resulted in a >100-fold increase in skeletal fatigue resistance, with resistance being exponentially related to the structural properties of the ulna.

The current findings indicate that an exercise program aimed at modifying the structural properties of the skeleton may be used as a possible prevention strategy for stress fractures. While extrinsic risk factors are undoubtedly more amenable to modification, bone is a dynamic tissue that can adapt its structural properties in response to exercise.[35–40] This has most commonly been shown in the growing skeleton[36,37,39,41]; however, exercise can also positively influence the structural properties of the adult skeleton.[35,38,40] Because stress fracture susceptibility is directly related to the structural properties of the skeleton,[18–21] exercise-induced enhancement of its structure may reduce the risk of stress fracture.

The use of exercise as a possible prevention strategy for stress fractures has previously been hypothesized[18,22–24] and has initial clinical support.[21,23,24] Milgrom et al.[23] showed, in three prospective epidemiological studies, that military recruits who played ball sports regularly for at least 2 years before basic training had less than one-half the risk of developing a stress fracture than recruits who did not play ball sports. Similarly, Lappe et al.[21] showed that a history of regular exercise in military recruits was protective

against stress fracture and that a longer history of exercise further decreased the relative risk. However, there is currently no prospective study showing that exercise-induced bone changes can reduce stress fracture occurrence.

In designing exercise programs to influence stress fracture risk, it must be remembered that, whereas repetitive mechanical loading can act as a potent anabolic stimulus,[25] it can also lead to skeletal fatigue. Therefore, exercise programs need to be designed to induce the desired changes in bone structure without inflicting harm in the form of microdamage generation and its accumulation. One method of achieving this is to ensure that exercise duration and, subsequently, the number of loading cycles to which a bone is exposed is restricted. For further details regarding exercise design for enhancing bone structure and strength, refer to recent reviews by Turner and Robling[26] and Warden et al.[27]

An interesting finding in this study was that large increases in ulna fatigue resistance could be generated with only small changes in its structural properties. This is consistent with previous studies showing that the mechanical properties of a bone can be greatly enhanced with only small changes in its structural properties.[29,42] This occurs as loading induces bone adaptation at biomechanically relevant sites. Axial compression of the rat ulna accentuates its mediolateral curvature to generate strain and subsequent adaptation in the mediolateral plane (Fig. 1). Because this plane corresponds with the plane of I_{MIN}, adaptation to the mechanical loading program was predominantly observed by an increase in I_{MIN}. By fatigue loading the ulnas in the same direction as they were adapted, the nearly 2-fold increase in I_{MIN} resulted in a >100-fold increase in fatigue resistance.

Adaptation to mechanical loading at biomechanically relevant sites enables a bone to better resist applied loads. This was confirmed in this study through strain calculations. Midshaft strains during fatigue testing in the same load group were one-third lower in loaded ulnas than nonloaded ulnas. Lower strain in adapted bones has implications for fatigue resistance because damage accumulation and subsequent fatigue failure in response to cyclic loading are threshold-driven[43] and occur more rapidly with higher strain.[44] To confirm the contribution of strain magnitude in determining fatigue resistance, a subgroup of loaded and nonloaded ulnas in this study underwent fatigue testing at the same strain magnitude. There was no significant difference in fatigue resistance in these ulnas, indicating that the material properties of the bones were similar.

The results of this study have a number of potential clinical implications. In addition to indicating that exercise may be used as a potential preventative strategy for stress fractures, the results confirm that the structural properties of the skeleton are important in determining its mechanical properties. Whereas fatigue resistance was correlated with the amount of material present, the distribution of this mineral was important. This indicates that assessment of bone geometry at a relevant skeletal site may provide a more accurate prediction of stress fracture risk in the clinical setting than sole assessment of the amount of bone present. Because mechanical loading generated a large increase in skeletal fatigue resistance despite only relatively small changes in its structural properties, this study also indicates that exercise programs aimed at modifying stress fracture risk may not need to generate large bone changes to have a significant impact on risk. This can be appreciated using clinical data. Bass et al.[36] showed that prepubertal tennis players have 11–14% greater polar moment of inertia ($I_P = I_{MAX} + I_{MIN}$) in their loaded humerus than nonloaded humerus. Based on our data, this relatively small side-to-side difference in I_P equates to a 2- to 4-fold increase in fatigue resistance in the loaded humerus. In terms of a site that is relevant to stress fracture, Marguiles et al.[38] showed that tibial aBMD increased by 5.2% in military recruits during a 4-month training period. This change equates to a 6-fold increase in fatigue resistance based on our data. Because fatigue resistance was exponentially negatively related to microstrain, any technique that reduces bone strain at relevant sites during loading will have a large impact on stress fracture risk. As an example, Milgrom et al.[45] showed that running on a treadmill reduced tibial axial compressive strain by 66% compared with overground running. Based on our data, this reduction in strain would equate to a 70-fold increase in fatigue resistance.

The findings of this study need to be considered in light of several limitations. The fatigue behavior of bone depends on how it is loaded. We fatigued specimens at relatively high initial peak strains. In the same load group, the initial peak strain in nonloaded ulnas averaged >5000 $\mu\varepsilon$. This compares to typical peak strains in the vicinity of 2000 $\mu\varepsilon$ measured during strenuous activities in humans[45,46]; however, it is in the range of strains measured in alternate species.[47] The use of supraphysiological strains was necessary because initial trials showed reproducing physiological strains required impracticably long fatigue tests. Test duration was also limited by loading ulnas at a supraphysiological frequency (5 Hz), which combined with the high strain, meant that the strain rates during testing were also supraphysiological. The ulnas were tested ex vivo, which meant that they were devitalized. This enabled strict study of the contribution of the material and structural properties of the skeleton to fatigue resistance. However, the ex vivo testing does limit the applicability of the findings to the in vivo situation where other intrinsic factors (such as muscle contributions to the loading environment and bone turnover) may significantly influence fatigue resistance.

In summary, we found that by enhancing the structural properties of a bone through a mechanical loading program, its fatigue resistance could be significantly improved. This indicates that exercise programs aimed at modifying bone structure may be used as a possible prevention strategy for stress fractures. These programs do not need to generate large bone changes at stress fracture relevant sites because fatigue resistance was found to be exponentially related to the structural properties of the skeleton.

ACKNOWLEDGMENTS

This work was supported by the U.S. Army Medical Research and Materiel Command (USAMRMC 03351012) to JL.

REFERENCES

1. Burr DB, Forwood MR, Fyhrie DP, Martin RB, Schaffler MB, Turner CH 1997 Bone microdamage and skeletal fragility in osteoporotic and stress fractures. J Bone Miner Res **12**:6–15.
2. Frost HM 1960 Presence of microscopic cracks in vivo in bone. Henry Ford Hosp Med Bull **8**:25–35.
3. Martin RB 2003 Fatigue microdamage as an essential element of bone mechanics and biology. Calcif Tissue Int **73**:101–107.
4. Burr DB 2002 Targeted and nontargeted remodeling. Bone **30**:2–4.
5. Bennell KL, Malcolm SA, Wark JD, Brukner PD 1996 Models for the pathogenesis of stress fractures in athletes. Br J Sports Med **30**:200–204.
6. Bennell KL, Brukner PD 1997 Epidemiology and site specificity of stress fractures. Clin Sports Med **16**:179–196.
7. Gillespie WJ, Grant I 2000 Interventions for preventing and treating stress fractures and stress reactions of bone of the lower limbs in young adults. Cochrane Database Syst Rev **2**:CD000450.
8. Bennell K, Matheson G, Meeuwisse W, Brukner P 1999 Risk factors for stress fractures. Sports Med **28**:91–122.
9. Carter DR, Hayes WC 1976 Fatigue life of compact bone. I. Effects of stress amplitude, temperature and density. J Biomech **9**:27–34.
10. Carter DR, Hayes WC 1976 Fatigue life of compact bone. II. Effects of microstructure and density. J Biomech **9**:211–218.
11. Armstrong DW III, Rue J-PH, Wilckens JH, Frassica FJ 2004 Stress fracture injury in young military men and women. Bone **35**:806–816.
12. Bennell K, Crossley K, Jayarajan J, Walton E, Warden S, Kiss ZS, Wrigley T 2004 Ground reaction forces and bone parameters in females with tibial stress fracture. Med Sci Sports Exerc **36**:397–404.
13. Bennell KL, Malcolm SA, Thomas SA, Ebeling PR, McCrory PR, Wark JD, Brukner PD 1995 Risk factors for stress fractures in female track-and-field athletes: A retrospective analysis. Clin J Sport Med **5**:229–235.
14. Carbon R, Sambrook PN, Deakin V, Fricker P, Eisman JA, Kelly P, Maguire K, Yeates MG 1990 Bone density of elite female athletes with stress fractures. Med J Aust **153**:373–376.
15. Crossley KM, Bennell KL, Wrigley T, Oakes B 1999 Ground reaction forces, bone characteristics, and tibial stress fracture in male runners. Med Sci Sports Exerc **31**:1088–1093.
16. Girrbach RT, Flynn TW, Browder DA, Guffie KL, Moore JH, Masullo LN, Bare AC, Bradley Y 2001 Flexural wave propagation velocity and bone mineral density in females with and without tibial bone stress injuries. J Orthop Sports Phys Ther **31**:54–62.
17. Lauder TD, Dixit S, Pezzin LE, Williams MV, Campbell CS, Davis GD 2000 The relation between stress fractures and bone mineral density: Evidence from active-duty army women. Arch Phys Med Rehabil **81**:73–79.
18. Beck TJ, Ruff CB, Mourtada FA, Shaffer RA, Maxwell-Williams K, Kao GL, Sartorius DJ, Brodine S 1996 Dual-energy X-ray absorptiometry derived structural geometry for stress fracture prediction in male U.S. Marine Corps recruits. J Bone Miner Res **11**:645–653.
19. Beck TJ, Ruff CB, Shaffer RA, Betsinger K, Trone DW, Brodine SK 2000 Stress fracture in military recruits: Gender differences in muscle and bone susceptibility factors. Bone **27**:437–444.
20. Bennell KL, Malcolm SA, Thomas SA, Reid SJ, Brukner PD, Ebeling PR, Wark JD 1996 Risk factors for stress fractures in track and field athletes: A twelve-month prospective study. Am J Sports Med **24**:810–818.
21. Lappe JM, Stegman MR, Recker RR 2001 The impact of lifestyle factors on stress fractures in female Army recruits. Osteoporos Int **12**:35–42.
22. Danova NA, Colopy SA, Radtke CL, Kalscheur VL, Markel MD, Vanderby R Jr, McCabe RP, Escarcega AJ, Muir P 2003 Degradation of bone structural properties by accumulation and coalescence of microcracks. Bone **33**:197–205.
23. Milgrom C, Simkin A, Eldad A, Nyska M, Finestone A 2000 Using bone's adaptation ability to lower the incidence of stress fractures. Am J Sport Med **28**:245–1.
24. Milgrom C, Finestone A, Novack V, Pereg D, Goldich Y, Kreiss Y, Zimlichman E, Kaufman S, Lierbergall M, Burr DB 2004 The effect of prophylactic treatment with risedronate on stress fracture incidence among infantry recruits. Bone **35**:418–424.
25. Turner CH, Robling AG 2004 Exercise as an anabolic stimulus for bone. Curr Pharm Des **10**:2629–2641.
26. Turner CH, Robling AG 2003 Designing exercise regimens to increase bone strength. Exerc Sport Sci Rev **31**:45–50.
27. Warden SJ, Fuchs RK, Turner CH 2004 Steps for targeting exercise towards the skeleton to increase bone strength. Eur Med Phys **40**:223–232.
28. Torrance AG, Mosley JR, Suswillo RFL, Lanyon LE 1994 Noninvasive loading of the rat ulna *in vivo* induces a strain-related modeling response uncomplicated by trauma or periosteal pressure. Calcif Tissue Int **54**:241–247.
29. Robling AG, Hinant FM, Burr DB, Turner CH 2002 Improved bone structure and strength after long-term mechanical loading is greatest if loading is separated into short bouts. J Bone Miner Res **17**:1545–1554.
30. Hsieh YF, Wang T, Turner CH 1999 Viscoelastic response of the rat loading model: Implications for studies of strain-adaptive bone formation. Bone **25**:379–382.
31. Kotha SP, Hsieh YF, Strigel RM, Muller R, Silva MJ 2004 Experimental and finite element analysis of the rat ulnar loading model-correlations between strain and bone formation following fatigue loading. J Biomech **37**:541–548.
32. Mosley JR, March BM, Lynch J, Lanyon LE 1997 Strain magnitude related changes in whole bone architecture in growing rats. Bone **20**:191–198.
33. Linn SK, Giles KE, Christiansen B, Roy ME, Cheverud J, Silva MJ 2005 Mouse bone mechanical testing—restoration of properties after long-term dried storage and comparison of material properties from femur vs. radius bending tests. In: Transactions of the 51st Annual Meeting of the Orthopaedic Research Society. Orthopaedic Research Society, Rosemont, IL, USA, p. 656.
34. Schriefer JL, Warden SJ, Saxon LK, Robling AG, Turner CH 2004 Cellular accommodation and the response of bone to mechanical loading. J Biomech (in press).
35. Adami S, Gatti D, Braga V, Bianchini D, Rossini M 1999 Site-specific effects of strength training on bone structure and geometry of ultradistal radius in postmenopausal women. J Bone Miner Res **14**:120–124.
36. Bass SL, Saxon L, Daly RM, Turner CH, Robling AG, Seeman E, Stuckey S 2002 The effect of mechanical loading on the size and shape of bone in pre-, peri-, and postpubertal girls: A study in tennis players. J Bone Miner Res **17**:2274–2280.
37. MacKelvie KJ, Petit MA, Khan KM, Beck TJ, McKay HA 2004 Bone mass and structure are enhanced following a 2-year randomized controlled trial of exercise in prepubertal boys. Bone **34**:755–764.
38. Margulies JY, Simkin A, Leichter I, Bivas A, Steinberg R, Giladi M, Stein M, Kashtan H, Milgrom C 1986 Effect of intense physical activity on the bone-mineral content in the lower limbs of young adults. J Bone Joint Surg Am **68**:1090–1093.
39. Petit MA, McKay HA, MacKelvie KJ, Heinonen A, Khan KM, Beck TJ 2002 A randomized school-based jumping intervention confers site and maturity-specific benefits on bone structural properties in girls: A hip structural analysis study. J Bone Miner Res **17**:363–372.
40. Uusi-Rasi K, Kannus P, Cheng S, Sievanen H, Pasanen M, Heinonen A, Nenonen A, Halleen J, Fuerst T, Genant H, Vuori I 2003 Effect of alendronate and exercise on bone and physical performance of postmenopausal women: A randomized controlled trial. Bone **33**:132–143.
41. Fuchs RK, Bauer JJ, Snow CM 2001 Jumping improves hip and lumbar spine bone mass in prepubescent children: A randomized controlled trial. J Bone Miner Res **16**:148–156.
42. Jarvinen TL, Kannus P, Sievanen H, Jolma P, Heinonen A,

Jarvinen M 1998 Randomized controlled study of effects of sudden impact loading on rat femur. J Bone Miner Res **13:**1475–1482.
43. Burr DB, Turner CH, Naick P, Forwood MR, Ambrosius W, Hasan MS, Pidaparti R 1998 Does microdamage accumulation affect the mechanical properties of bone? J Biomech **31:** 337–345.
44. Forwood MR, Parker AW 1989 Microdamage in response to repetitive torsional loading in the rat tibia. Calcif Tissue Int **45:**47–53.
45. Milgrom C, Finestone A, Segev S, Olin C, Arndt T, Ekenman I 2003 Are overground or treadmill runners more likely to sustain tibial stress fracture? Br J Sports Med **37:**160–163.
46. Burr DB, Milgrom C, Fyhrie D, Forwood M, Nyska M, Finestone A, Hoshaw S, Saiag E, Simkin A 1996 In vivo measurement of human tibial strains during vigorous activity. Bone **18:**405–410.
47. Nunamaker DM, Butterweck DM, Provost MT 1990 Fatigue fractures in thoroughbred racehorses: Relationships with age, peak bone strain, and training. J Orthop Res **8:**604–611.

Address reprint requests to:
Stuart J Warden, PhD
Department of Physical Therapy
School of Health and Rehabilitation Sciences
Indiana University
1140 W. Michigan Street, CF-326
Indianapolis, IN 46202, USA
E-mail: stwarden@iupui.edu

Received in original form September 29, 2004; revised form November 5, 2004; accepted December 14, 2004.

LIPPINCOTT WILLIAMS & WILKINS

MEDICINE & SCIENCE IN SPORTS & EXERCISE®

Official Journal of the American College of Sports Medicine

©2005The American College of Sports Medicine Volume 37(5) Supplement, May 2005, p S452

Exercise-induced Bone Adaptation Significantly Increases Skeletal Fatigue Resistance: 2341 11:00 AM – 11:15 AM

[**G-35**: Free Communication/Slide – **Bone Responses to Training**: SATURDAY, JUNE 4, 2005 10:45 AM - 12:15 PM ROOM: Jackson A]

Warden, Stuart J.; Hurst, Julie A.; Sanders, Megan S.; Turner, Charles H.; Burr, David B.; Li, Jiliang

Indiana University, Indianapolis, IN.
Email: stwarden@iupui.edu

PURPOSE

Stress fractures are particularly common among athletes and military recruits, and have ramifications in terms of morbidity and time lost from participation. Despite their significance, there are currently limited preventative strategies for stress fractures. As stress fracture risk is directly influenced by skeletal properties (such as bone mass and size), it has been hypothesized that modification of these properties using an exercise program may positively influence risk. Bone is inherently mechanosensitive, and responds and adapts to its mechanical environment. The aim of this study was to investigate whether the bone changes associated with a mechanical loading program can enhance skeletal fatigue resistance.

METHODS

Site-specific mechanical loading was performed on one forearm of adult female Sprague-Dawley rats using the axial compression loading model. Loading was performed three days per week for five consecutive weeks to induce adaptation. The loaded and non-loaded ulnas in each animal were removed following the loading program, and their material and structural properties determined. The ulna pairs were subsequently loaded until fatigue failure at the same constant peak axial load.

RESULTS

Loading induced consistent and predictable changes in the structural properties of loaded ulnas, with the largest change being a nearly two-fold increase in midshaft minimum second moment of area (I_{MIN}). The mechanical-loading induced bone changes resulted in a more than 100-fold increase in fatigue resistance in loaded ulnas, with resistance being exponentially related to the structural properties of the ulna.

CONCLUSIONS

This study found that by enhancing the structural properties of a bone via a mechanical loading

program its fatigue resistance could be significantly improved. This indicates that an exercise program aimed at modifying bone structure may be used as a possible prevention strategy for stress fractures. As large increases in fatigue resistance were generated with only small changes in its structural properties, such a program would not need to generate large bone changes to have a significant impact on stress fracture risk. Based on our data, an increase of 5% in bone mineral content would equate to a 6-fold increase in fatigue resistance. Similarly, as fatigue resistance was exponentially negatively related to strain any technique that reduces bone strain during loading will have a large impact on stress fracture risk. Running on a treadmill has been shown to reduce tibial axial compressive strain by 66% compared to overground running. Based on our data, this reduction in strain would increase fatigue resistance by 70-fold.

Accession Number: 00005768-200505001-02341

BONE ADAPTATION TO A MECHANICAL LOADING PROGRAM SIGNIFICANTLY INCREASES SKELETAL FATIGUE RESISTANCE

+*Warden, S J; *Hurst, J A; *Sanders, M S; *Turner, C H; *Burr, D B; *Li, J
+*Indiana University School of Medicine, Indianapolis, IN
stwarden@iupui.edu

INTRODUCTION: A stress fracture represents the failure of a bone to withstand repetitive bouts of mechanical loading. Despite the clinical significance of stress fractures in terms of loss of training and competition time, there are few effective preventative strategies. One hypothesized method is to use an exercise program to alter the material and structural properties of an at risk bone. Bone is inherently mechanosensitive and adapts its properties in response to the prevailing mechanical environment. By inducing adaptation through a mechanical loading program, a bone's resistance to fatigue may be enhanced resulting in a subsequent reduction in stress fracture risk. However, the ability of a loading program to reduce stress fracture risk has not been established. The aim of this study was to investigate whether the material and structural adaptation of bone to a mechanical loading program can improve skeletal fatigue resistance in an anim al model.

METHODS: Adult female Sprague-Dawley rats (250-300g) were used, and all procedures were approved by an Institutional Animal Care and Use Committee. Site-specific mechanical loading was achieved using the ulna axial compression loading model, with the animals under isoflurane anesthesia (Abbott Laboratories, North Chicago, IL). This mode of loading accentuates the mediolateral curvature of the ulna and translates most (approximately 90%) of the axial load into a bending moment to create a strain distribution similar to that resulting from normal limb usage during locomotion. Loading was applied using a 2-Hz haversine waveform for 360 cycles/day, three days per week for five consecutive weeks. The peak load magnitude was 17 N, which elicits a compressive strain of approximately 3600 $\mu\varepsilon$ on the medial surface of the ulna midshaft. Left ulnas served as an internal control and were not loaded. Normal cage activity was allowed between loading sessions. Animals were killed five weeks following the final loading session.

Adaptation to mechanical loading was determined by assessing both the material and structural properties of each ulna. Material properties were assessed using dual energy X-ray absorptiometry (DXA) and peripheral quantitative tomography (pQCT). DXA was performed to collect whole ulna bone mineral content (BMC; mg) and areal bone mineral density (aBMD; $g.cm^{-2}$) data, whereas pQCT was performed to determine ulna midshaft BMC ($mg.cm^{-1}$) and volumetric BMD (vBMD; $mg.cm^{-3}$). Structural properties of each ulna midshaft were derived from micro-computed tomography (μCT) slices. Slice images were imported into Scion Image wherein ulna midshaft cortical area (Ct.Ar; mm^2), and the maximum (I_{MAX}; mm^4) and minimum (I_{MIN}; mm^4) second moments of area were determined. In addition, the section diameter (Se.Dm; mm) of each ulna was determined as the largest diameter of the bone in the plane parallel to the I_{MIN} axis.

To permit the calculation of microstrain ($\mu\varepsilon$), right (loaded) and left (non-loaded) ulnas from four animals chosen at random were used for a load-strain calibration experiment. A single element strain gauge (EA-06-015DJ-120; Measurements Group, Inc., Raleigh, NC) was bonded at the midpoint of each dna, and the ulnas were axially loaded at four different peak loads. The peak-to-peak gauge voltage was converted to strain, and a graph was constructed plotting $\mu\varepsilon/N$ versus c/I_{MIN}, where c is 2/3 of the Se.Dm. The slope of this graph (0.018 $\mu\varepsilon/N/mm^{-3}$) was used to predict strain during fatigue testing in experimental ulnas from their I_{MIN} and c using the derived equation:

$$\mu\varepsilon = \frac{N \times c}{0.018 \times I_{MIN}}$$

Remaining ulna pairs were loaded at a constant peak load of 25 N until fatigue failure. For testing, ulnas were fixed with 0.5 N of preload between two opposing cup-shaped platens on an electromagnetic actuator (Bose® ElectroForce® 3200 series; EnduraTEC, Minnetonka, MN) and axially loaded in load control. Loading was performed continuously in a room temperature saline bath using a 5 Hz haversine waveform. Upon fatigue failure the number of completed cycles was recorded for each bone.

RESULTS: The mechanical loading program had predictable and consistent effects on the material and structural properties of the ulna, with loaded ulnas having significantly greater values for all measurements compared to the contralateral non-loaded ulnas (Fig. 1). The largest difference was observed for I_{MIN}, which was near two-fold greater in exercised ulnas. As a result of the adaptation in loaded ulnas, they experienced only 3614 ± 409 $\mu\varepsilon$ when loaded at 25 N during fatigue testing, which compared to the 5361 ± 618 $\mu\varepsilon$ experienced by nonloaded ulnas ($p < 0.05$, paired t-test).

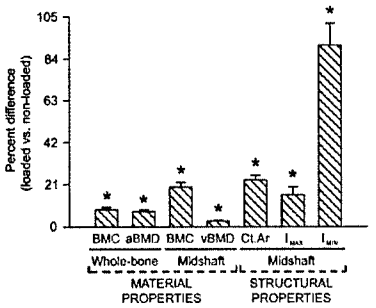

Fig. 1. Effect of exercise on the material and structural properties of the ulna. *Indicates significant difference from 0% (no difference between loaded and non-loaded ulnas) ($p < 0.05$; single sample t-test with population mean of 0%). Error bars represent ± 1 SE.

The material and structural adaptation of the ulna to mechanical loading significantly increased ulna fatigue resistance. Loaded ulnas failed in fatigue after 1.3 million cycles, compared to the 16,850 cycles required for non-loaded ulnas (Fig. 2). This represents a 80-fold increase in ulna fatigue resistance resulting from the mechanical loading-induced bone adaptation.

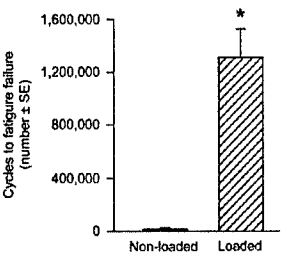

Fig. 2. Effect of exercise-induced bone changes on ulna fatigue resistance. *Indicates significant difference from non-loaded ulna ($p < 0.01$, paired t-test). Error bars represent ± 1 SE.

DISCUSSION: By inducing adaptation of its material and structural properties, a mechanical loading program increased the fatigue resistance of the rat ulna by 80-fold. This large increase occurred despite relatively low gains in aBMD and BMC because load-induced new bone was localized to biomechanically relevant sites. Axial compression of the rat ulna accentuates its mediolateral curvature to generate strain and subsequent adaptation in the mediolateral plane. As this plane corresponds with the plane of I_{MIN}, adaptation to the mechanical loading program was predominantly observed as an increase in I_{MIN}. By fatigue loading the ulnas in the same direction as they were adapted, the two-fold increase in I_{MIN} resulted in a substantial increase in fatigue resistance.

FUNDING SOURCE: U. S. Army Medical Research and Materiel Command (USAMRMC #03351012)

EFFECT OF LOW INTENSITY PULSED ULTRASOUND AND A CYCLO-OXYGENASE-2 INHIBITOR ON STRESS FRACTURE REPAIR

+*Li, J; *Warden, S J; *Waugh, L; *Burr, D B
+Indiana University School of Medicine, Indianapolis, IN
jilili@iupui.edu

Introduction

Stress fracture is one of the most common injuries in military training and sports. Stress fractures are repaired through bone remodeling process. Nonsteroidal anti-inflammatory drugs, such as cyclooxygenase-2 (COX-2) inhibitors, are commonly used to treat pain and inflammation associated with stress fracture. But it is not clear whether COX-2 inhibitors may affect remodeling during stress fracture repair. Although low intensity pulsed ultrasound (LIPUS) has been shown to accelerate fracture healing, whether LIPUS influences bone healing is the presence of COX-2 inhibitors is unknown. The goal of this study was to test the effect of LIPUS and COX-2 inhibitors alone and in combination on stress fracture repair.

Materials and Methods

Bilateral stress fractures were induced in the ulnas of 48 adult female Sprague-Dawley rats. Rats were anaesthetized with an intramuscular injection of ketamine hydrochloride (50 mg/kg) and xylazine (10 mg/kg). One bout of axial compressive loading was applied on ulnas using a load-controlled electromagnetic device. Loading had a peak magnitude of 17- 20 N (~3600 microstrain at mid-ulna) which was introduced at a frequency of 2 Hz for 4000-6000 cycles. The loading was stopped when the displacement increased 10% (equivalent to 10% loss of stiffness), as monitored using a CCD Laser Displacement Sensor.

Beginning the first day following stress fracture induction, half of the animals were given celebrex (a specific COX-2 inhibitor) by gavage at a dose of 4 mg/kg/day. The remaining animals were given vehicle (polyethylene glycol solution). In addition, all animals had their forelimbs shaved, and were treated unilaterally with active-LIPUS (active ultrasound) and contralaterally with inactive-LIPUS (placebo) while animals were anaesthetized using isoflurane inhalation (1-3%). Active-LIPUS consist of a 200-μs burst of 1.5-MHz sine waves repeating at 1-kHz. The I_{SATA} was set at 100 mW/cm^2. Active- and inactive-LIPUS was coupled with the skin using standard ultrasound gel and was introduced daily for 20-minutes. Therefore, a total of 4 groups were generated based on the combinations of celebrex and LIPUS treatments: Vehicle, Vehicle+LIPUS, Celebrex and Celebrex+LIPUS groups. Equal numbers of animals from each group were sacrificed at 2, 4 and 8 weeks following stress fracture induction. Three and nine days prior to sacrifice intraperitoneal injections of calcein (7 mg/kg, Sigma Chemical Co., St. Louis, MO) were administered. Following sacrifice, ulnas were dissected free and bone mineral content and density were measured using a PIXImus densitometer. The ulnas were then prepared for histological analysis using *en bloc* basic fuchsin staining. Histomorphometric measurements were performed on cross sections of the midshaft ulna.

Data are expressed as mean±SEM (standard error of the mean). Differences among group means were tested for significance by two-way ANOVA with one repeated measurement at each time point.

Results

Periosteal woven bone formation on the periosteal surface resulted from fatigue loading. There was no difference in woven bone area or bone mineral density among all the groups (Figure 1). Cracks were seen in the cortex of all ulnas and there was no difference in crack length among the groups. Bone resorption spaces around the crack were seen in all the ulnas at 2 weeks following fatigue loading (Figure 2). The maximum area of introcortical resorption spaces was found at 4 weeks. The sizes of resorption spaces decreased significantly at 8 weeks in all groups. There was no difference in area of resorption spaces at each time point among the groups.

There were no significant interactions between LIPUS and celebrex on intracortical bone formation rate (BFR) at any time point (all $p > 0.05$, Figure 3). However, at 4 and 8 weeks there was a significant LIPUS main effect on BFR (all $p < 0.05$), indicating a beneficial LIPUS effect. There was no main effect for celebrex at 4 weeks; however, such an effect existed at 8 weeks, indicating that celebrex significantly reduced BFR.

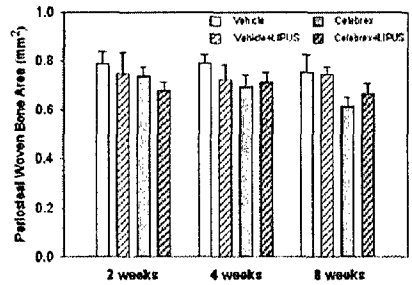

Figure 1. Area of woven bone formed in response to fatigue loading was not different among groups.

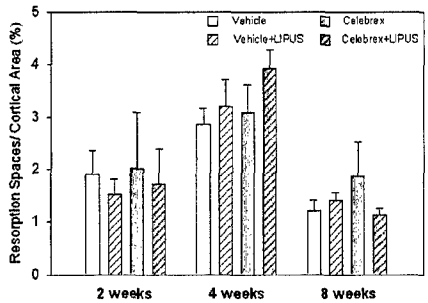

Figure 2. Intracortical bone resorption increased significantly in all groups until 4 weeks after production of bone cracks, but then decrease at 8 weeks. No difference was seen among the groups at each time point.

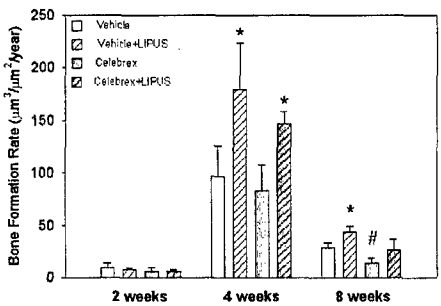

Figure 3. LIPUS significantly enhanced intracortical bone formation rate in the cortex during stress fracture repair (* $p < 0.05$ vs. Vehicle or Celebrex) at 4 and 8 weeks. Celebrex decreased bone formation (# $p < 0.05$ vs. Vehicle) at 8 weeks.

Discussion

This study indicates that LIPUS has a beneficial and celebrex has a detrimental effect on stress fracture repair. While neither LIPUS or celebrex influenced bone resorption, both had significant effects on intracortical BFR. These effects were opposing, and indicate that LIPUS may be used to facilitate stress fracture repair whereas celebrex may delay tissue level repair of stress fractures. There were no interactions between LIPUS and celebrex, indicating that the beneficial LIPUS effect was not mediated by a COX-2 pathway. These findings have implications for the clinical utility of these interventions in the management of stress fractures.

Funding Source: U. S. Army Medical Research and Materiel Command (USAMRMC #03351012)